
NUMERICAL SOLUTION OF STIFF ORDINARY DIFFERENTIAL EQUATIONS WITH RANDOM PROJECTION NEURAL NETWORKS

A PREPRINT

Evangelos Galaris

Dipartimento di Matematica e Applicazioni “Renato Caccioppoli”
Università degli Studi di Napoli Federico II
Napoli, Italy
evangelos.galaris@unina.it

Francesco Calabrò

Dipartimento di Matematica e Applicazioni “Renato Caccioppoli”
Università degli Studi di Napoli Federico II
Napoli, Italy
calabro@unina.it

Daniela di Serafino

Dipartimento di Matematica e Applicazioni “Renato Caccioppoli”
Università degli Studi di Napoli Federico II
Napoli, Italy
daniela.diserafino@unina.it

Constantinos Siettos *

Dipartimento di Matematica e Applicazioni “Renato Caccioppoli”
Università degli Studi di Napoli Federico II
Napoli, Italy
constantinos.siettos@unina.it

August 4, 2021

ABSTRACT

We propose a numerical scheme based on Random Projection Neural Networks (RPNN) for the solution of Ordinary Differential Equations (ODEs) with a focus on stiff problems. In particular, we use an Extreme Learning Machine, a single-hidden layer Feedforward Neural Network with Radial Basis Functions which widths are uniformly distributed random variables, while the values of the weights between the input and the hidden layer are set equal to one. The numerical solution is obtained by constructing a system of nonlinear algebraic equations, which is solved with respect to the output weights using the Gauss-Newton method. For our illustrations, we apply the proposed machine learning approach to solve two benchmark stiff problems, namely the Rober and the van der Pol ones (the latter with large values of the stiffness parameter), and we perform a comparison with well-established methods such as the adaptive Runge-Kutta method based on the Dormand-Prince pair, and a variable-step variable-order multistep solver based on numerical differentiation formulas, as implemented in the `ode45` and `ode15s` MATLAB functions, respectively. We show that our proposed scheme yields good numerical approximation accuracy without being affected by the stiffness, thus outperforming in some cases the `ode45` and `ode15s` functions. Importantly, upon

*Corresponding author

training using a fixed number of collocation points, the proposed scheme approximates the solution in the whole domain in contrast to the classical time integration methods.

Keywords Machine Learning · Random Projection Neural Networks · Radial Basis Functions · Stiff ODEs

1 Introduction

The idea of using Artificial Neural Networks (ANNs) for the numerical solution of Ordinary Differential Equations (ODEs) dates back to the '90s. One of the first works in the field was proposed by Lee and Kang [44], who addressed a modified Hopfield Neural Network to solve a first-order nonlinear ODE. This method is based on the discretization of the differential operator with finite differences and the minimization of an energy function of the resulting algebraic difference equations. Following up this work, Meade and Fernandez [50] used a non-iterative scheme based on Feed-forward Neural Networks (FNN) for the solution of linear ODEs, where the estimation of the weights of the FNN is based on the Galerkin weighted-residuals method. In 1998, Lagaris et al. [42] introduced a numerical optimization method based on FNNs for the solution of nonlinear ODEs and PDEs. The method constructs appropriate trial functions by the aid of a single-hidden layer FNN that is trained to minimize the error between the FNN prediction and the right-hand side of the differential equations. The proposed approach is demonstrated through both initial and boundary-value problems and a comparison with Galerkin finite elements is also provided. Based on the work of Lagaris et al. [42], Filici [23] proposed a single-layer multiple linear output perceptron, providing a proof for the error bound. Network training was performed with the LMDER optimization solver from MINIPACK. The performance of the approach was tested through simple ODE problems, including the van der Pol equation, but without stiffness. Tsoulos et al. [68] employed an FNN trained by grammatical evolution and a local optimization procedure to solve second-order ODEs. More recently, Dufera [18] addressed a deep training network with back-propagation. The performance of the approach was tested with the non-stiff ODEs presented in Lagaris et al. [42]. The authors report that their scheme outperforms the non-adaptive 4th order Runge-Kutta method in terms of numerical approximation accuracy when considering short time intervals and a small number of collocation points. A review and presentation of various ANN schemes for the solution of ODEs can be found in Yadav et al. [73]. In all the above procedures, a computationally demanding optimization algorithm is required for the evaluation of the parameters of the network and the ODEs problems are non-stiff.

Yang et al. [74] aim to solve ODE problems using the so-called Extreme Learning Machine (ELM) concept [29, 31]: the weights between the input and the hidden layer, as well as the biases of the hidden nodes, are chosen randomly, and the remaining unknown weights between the hidden and the output layer are computed in one step using least squares with regularization. The authors address a single-layer Legendre neural network to solve non-stiff ODEs up to second order, including the Emden-Fowler equation. The performance of the scheme is compared against other machine learning schemes, including a cosine basis function neural network trained by the gradient descent algorithm, the explicit Euler scheme, the Suen 3rd-order and the classical 4th-order Runge-Kutta methods. The authors report high numerical accuracy and computing times comparable or smaller than the other methods.

As discussed, the above studies deal with non-stiff ODE problems. One of the first papers that dealt with the solution of stiff ODEs and Differential-Algebraic Equations by ANNs was that of Gerstberger and Rentrop [24], where an FNN architecture was proposed to implement the implicit Euler scheme. The performance of that architecture was demonstrated using scalar ODEs and the van der Pol equations considering however only mild stiffness, setting the parameter that controls the stiffness to values up to 5.

More recently, theoretical and technological advances have renewed the interest for developing and applying machine learning techniques for the solution of differential equations. Due to the fact that (large-scale systems of) stiff ODEs arise in modelling an extremely wide range of problems, from biology and neuroscience to engineering processes and chemical kinetics, and from financial systems to social science and epidemiology, there is a re-emerging interest in developing new methods for their efficient numerical solution. Mall and Chakraverty [49] proposed a single-layer Hermite polynomial-based neural network trained with back-propagation to approximate the solutions of the van der Pol-Duffing and Duffing oscillators with low to medium values of the stiffness parameter. Following up this work, Chakraverty and Mall [12] proposed a single-layer Chebyshev neural network with regression-based weights to solve first- and second-order nonlinear ODEs and in particular the nonlinear Lane-Emden equation. The training was achieved using back-propagation. Budkina et al. [7] and Famelis and Kaloutsas [22] proposed a single-layer ANN to solve highly stiff ODE problems. The networks were trained for different values of the parameter that controls stiffness over relatively short time intervals using the Levenberg-Marquardt algorithm. The above studies on the solution of stiff ODEs report good numerical approximation accuracy of the proposed schemes, in general for relatively short time intervals and small sizes of the grid. However, no indication is given about the computational time required for the training versus the time required by widely used solvers for low-to-medium and medium-to-high stiff problems

such as the `ode45` and `ode15s` functions available from the MATLAB ODE suite [67]. We note that the previous approaches, in general, fit into the framework of Physics-Informed Neural Networks (PINNs), which are trained to solve supervised learning tasks while respecting any given laws of physics described by general nonlinear differential equations [39, 60]. This is also part of the so-called scientific machine learning, which is emerging as a potential alternative to classical scientific computing.

1.1 Our Contribution

We propose a new scheme based on Random Projection Neural Networks (RPNNs) and in particular on ELMs. RPNNs are a family of networks including randomized and Random Vector Functional Link Networks (RVFLNs) [34, 53, 65], Echo-State Neural Networks and Reservoir Computing [36, 37, 52, 55, 64], and Extreme Learning Machines [29, 30, 31]. The keystone idea behind all these approaches is to use a fixed-weight configuration between the input and the hidden layer, fixed biases for the nodes of the hidden layer, and a linear output layer. Hence, the output is projected linearly onto the functional subspace spanned by the nonlinear basis functions of the hidden layer, and the only unknowns that have to be determined are the weights between the hidden and the output layer. Their estimation is done in one step using least squares. Here, for the solution of stiff problems of ODEs, we propose a single-layer FNN with Radial Basis Functions (RBFs) whose parameters are properly uniformly-distributed random variables. Thus, the proposed neural network scheme constitutes a Lipschitz embedding constructed through the random projection. The feasibility of the scheme is guaranteed by the celebrated Johnson and Lindenstrauss Lemma [38] and universal approximation theorems proved for random projection networks, and in particular for ELMs [32].

By combining this choice of the underlying functional space, for which we can also explicitly compute the derivatives, and the Gauss-Newton method for the solution of the system of nonlinear algebraic equations equivalent to the least squares problem, we obtain an efficient way to calculate by collocation a neural network function that approximates the exact solution in any point of the domain. It is very important to mention that once the random parameters are chosen in a proper interval, the underlying space is capable to catch the steep gradient behaviours of the solution, thus providing good numerical accuracy also for stiff ODE problems and outperforming in some cases the `ode45` and the stiff solver `ode15s`: no adaptive strategy on the step size is needed so that the method can be used “as it is” despite the stiffness (see also what was demonstrated for boundary-layer problems with steep gradients in [9, 21]).

We apply the proposed scheme to solve two benchmark stiff ODE problems, namely the ROBER problem, a stiff system of three nonlinear ODEs describing the kinetics of an autocatalytic reaction [63], and the well-known van der Pol equations with high stiffness. We test the performance of the scheme, in terms of both approximation accuracy and computational time. We show that the proposed scheme performs comparably to, and in some cases where steep gradients arise better than, the `ode15s` in terms of numerical approximation accuracy, while `ode45` in some cases completely fails or needs many points to satisfy a specific tolerance. Moreover, our approach provides the solution directly as a function that can be evaluated at every point of the domain, in contrast to the classical numerical methods, where extra interpolation/extrapolation steps are usually performed for this purpose.

The structure of the paper is as follows. In Section 2 we give very briefly a coarse definition of stiff ODEs. In Section 3, we provide some preliminaries on the solution of ODEs with FNNs based on the “classical” optimization approach, and the basic concept behind the use of RPNNs; we also discuss the celebrated Johnson and Lindenstrauss Lemma [38]. In Section 4, we propose our approach for solving ODEs with RPNNs, providing also a pseudo-code of the corresponding algorithm, and discuss its approximation properties within the framework of the universal approximation theorem of ELMs [32]. In section 5, we present the numerical results obtained by applying the proposed approach to the above-mentioned low-dimensional stiff ODE problems (Rober and van der Pol problems) along with a comparison with `ode45` and `ode15s`. Conclusions are given in Section 6.

2 Stiff ODEs

We aim to solve initial-value ODE problems:

$$\begin{cases} \frac{dy_i}{dx} &= f_i(x, y_1, y_2, \dots, y_m), & i = 1, 2, \dots, m, \\ y_i(x_0) &= \alpha_i, \end{cases} \quad (1)$$

where the functions f_i and the values α_i are the input data, and the functions $y_i(x)$ are the unknowns. In order to simplify the notation, we group the functions $y_i(x)$ in a vector function $\mathbf{y}(x) : \mathbb{R} \rightarrow \mathbb{R}^m$, and the functions $f_i(x, y_1, y_2, \dots, y_m)$ in $\mathbf{f}(x, \mathbf{y})$.

The unknown solution can exhibit a complex behaviour, including steep gradients, which result in difficulties for the design and implementation of numerical methods. These difficult problems are usually the ones where the so-called stiffness arises. Until now, there is no complete and precise definition for stiffness. Following Lambert ([43]), one has

to consider stiffness as a phenomenon exhibited by the system rather than a property of it. Generally, an ODE problem is called stiff if there exists a solution that varies very slowly but there are nearby solutions that vary rapidly, so that (explicit) numerical algorithms need many small steps to obtain accurate and reliable results.

A widely used definition for stiffness is the following, given by J.D. Lambert (see also [6]):

If a numerical method with a finite region of absolute stability, applied to a system with any initial conditions, is forced to use in a certain interval of integration a step length which is excessively small in relation to the smoothness of the exact solution in that interval, then the system is said to be stiff in that interval.

In the case of constant coefficients, where the stiffness ratio is introduced, one can define stiffness as follows. Consider the linear constant coefficient inhomogeneous system in the unknown $\mathbf{y} : \mathbb{R} \rightarrow \mathbb{R}^m$:

$$\frac{d\mathbf{y}}{dx} = A\mathbf{y} + \overline{\mathbf{f}}(x), \quad (2)$$

where $\overline{\mathbf{f}} : \mathbb{R} \rightarrow \mathbb{R}^m$ is a nonlinear term and $A \in \mathbb{R}^{m \times m}$ is a constant and diagonalizable matrix with eigenvalues $\lambda_l \in \mathbb{C}$, $l = 1, 2, \dots, m$, (assumed distinct) and corresponding eigenvectors $\mathbf{c}_l \in \mathbb{C}^m$. Suppose also that:

$$\operatorname{Re}(\lambda_l) < 0, \quad l = 1, 2, \dots, m. \quad (3)$$

Definition 2.1 (Stiffness ratio). *With the above notations, let $\overline{\lambda}, \underline{\lambda} \in \{\lambda_l, l = 1, 2, \dots, m\}$ be such that*

$$|\operatorname{Re}(\overline{\lambda})| \geq |\operatorname{Re}(\lambda_l)| \geq |\operatorname{Re}(\underline{\lambda})|, \quad l = 1, 2, \dots, m.$$

We define the stiffness ratio of system (2) as

$$\frac{|\operatorname{Re}(\overline{\lambda})|}{|\operatorname{Re}(\underline{\lambda})|}.$$

The above definition is motivated by the explicit general solution of (2), that is

$$\mathbf{y}(x) = \sum_{l=1}^m \kappa_l \exp(\lambda_l x) \mathbf{c}_l + \mathbf{g}(x), \quad (4)$$

where $\mathbf{g}(x)$ is a particular integral taking into account the forcing term. In the hypothesis that (3) holds true, one has that each of the terms $\exp(\lambda_l x) \mathbf{c}_l$ vanishes as $x \rightarrow \infty$, and hence the solution $\mathbf{y}(x)$ approaches $\mathbf{g}(x)$ asymptotically as $x \rightarrow \infty$. In this case, the term $\exp(\lambda_l x) \mathbf{c}_l$ decays monotonically if λ_l is real, and sinusoidally if λ_l is complex. Interpreting x to be time (as it is often in physical problems), $\sum_{l=1}^m \kappa_l \exp(\lambda_l x) \mathbf{c}_l$ is called the transient solution and $\mathbf{g}(x)$ the steady-state solution. If $|\operatorname{Re}(\lambda_l)|$ is large, then the corresponding term $\kappa_l \exp(\lambda_l x) \mathbf{c}_l$ decays quickly as x increases and thus it is called a fast transient; if $|\operatorname{Re}(\lambda_l)|$ is small, then $\kappa_l \exp(\lambda_l x) \mathbf{c}_l$ decays slowly and is called a slow transient. Letting \overline{l} and \underline{l} be the indices identifying $\overline{\lambda}$ and $\underline{\lambda}$, respectively, we have that $\kappa_{\overline{l}} \exp(\overline{\lambda} x) \mathbf{c}_{\overline{l}}$ is the fastest transient and $\kappa_{\underline{l}} \exp(\underline{\lambda} x) \mathbf{c}_{\underline{l}}$ the slowest. The ratio between these two terms gives the stiff behaviour of the linear ODE system.

Many examples of stiff problems exhibit also other features, but for each feature there maybe other stiff problems not exhibiting that particular feature. However, we note that Lambert refers to these features as “statements” rather than definitions. A few of them are the following: (1) a linear constant coefficient system is stiff if all of its eigenvalues have negative real part and the stiffness ratio is large; (2) stiffness occurs when stability requirements, rather than those of accuracy, constrain the step length; and (3) stiffness occurs when some components of the solution decay much more rapidly than others. One could also say that stiffness is a numerical efficiency issue since non-stiff methods can in theory solve stiff problems if they use many points (i.e. a lot of computing time). In practice, many extremely stiff problems bias “classical” numerical methods to tiny steps, thus making the computational cost huge and hence the methods inapplicable. Furthermore, in some contexts, a specific number of points is available and as a consequence, the problem is unsolvable with several numerical methods.

3 Preliminaries

3.1 Feedforward Neural Networks

A FNN is a biologically inspired regression (or classification) algorithm. It consists of processing units, called neurons or nodes, organised in layers. There are three types of layers: the input layer, the output layer and possibly one or

more hidden layers. The units of the output and every hidden layer are connected to all the units of the previous layer. These connections may have different strengths, called weights, and encode the “knowledge” of the network. The data enter the input layer and pass through each layer during the forward phase. Each unit accepts a signal consisting of a (usually linear) combination of the outputs of the previous layer units and, using an activation function, creates an output that is transmitted to the next layer until the final output layer. Different activation functions and/or numbers of units can be used for each layer. A simple example of FNN is the Single Layer FNN (SLFNN), consisting of d input units, a single layer with h hidden units with biases, and k output units (without biases). Given an input $\mathbf{x} \in \mathbb{R}^d$, the output $\mathbf{N}(\mathbf{x}) \in \mathbb{R}^k$ of this SLFNN reads:

$$\mathbf{N}(\mathbf{x}) = W^o \Phi(W\mathbf{x} + \mathbf{b}, \mathbf{q}), \quad (5)$$

where $W^o = [w_{jl}^o] \in \mathbb{R}^{k \times h}$ is the matrix containing the weights from the hidden layer to the output layer, $\Phi : \mathbb{R}^h \times \mathbb{R}^s \rightarrow \mathbb{R}^h$ is a vector function with components h activation functions Φ_j , $W = [w_{ij}] \in \mathbb{R}^{h \times d}$ is the matrix containing the weights from the input to the hidden layer, $\mathbf{b} \in \mathbb{R}^h$ is the vector of the biases of the hidden nodes, and $\mathbf{q} \in \mathbb{R}^s$ is a vector containing the hyperparameters of the neural network, such as the parameters of the activation functions (e.g., for radial basis functions, the biases of the hidden neurons and the variances of the Gaussian functions), the learning rate, and the batch size. Many results are available concerning the approximation properties of the previous FNN. The most important one from the numerical point of view is the Universal Approximation Theorem, for which we refer to the original papers [14, 27, 28, 56] and the recent review [41]. Next we present some results concerning our proposed machine learning scheme. What can be summarized here is that a FNN is capable of approximating uniformly any (piecewise-)continuous (multivariate) function, to any desired accuracy. This implies that any failure of a function mapping by a (multilayer) network must arise from an inadequate choice of weights and biases or an insufficient number of hidden nodes. Moreover, in the univariate case only one hidden layer is needed.

Given a training set of n input-output pairs, the estimation of the appropriate weights and biases is usually attempted by using an optimization procedure aimed at minimizing a cost function. In particular, the “classical way” (see e.g. [42]) to solve (partial) differential equations in a d -dimensional domain with FNNs involves the solution of a minimization problem as follows. One first defines a trial solution in the form of

$$\Psi(\mathbf{x}, P, \mathbf{q}) = \Omega(\mathbf{x}, \mathbf{N}(\mathbf{x}, P, \mathbf{q})), \quad (6)$$

where $\Psi(\mathbf{x}, P, \mathbf{q})$ has m components, each associated with a component y_i of the solution \mathbf{y} , $\Omega : \mathbb{R}^d \times \mathbb{R}^k \rightarrow \mathbb{R}^m$ is sufficiently smooth, $\mathbf{N}(\mathbf{x}) = \mathbf{N}(\mathbf{x}, P, \mathbf{q})$ has k components $N_i(\mathbf{x}, \mathbf{p}_i, \mathbf{q})$, and P is a matrix containing the network parameters W^o , W and the vector of biases \mathbf{b} associated with the i th component of $\Psi(\mathbf{x}, P, \mathbf{q})$. Then, we consider a discretization of the equation that has to be solved, so as to settle the conditions that the optimization has to manage.

In the case of the solution of ODEs, according to the above notation $d = 1$, i.e. the input domain is one-dimensional (representing for example time). By discretizing the domain of the ODE problem (1) with n points $x_l \in \mathbb{R}$, so as to collocate the equations, one can determine the values of the network parameters in \mathbf{p} by solving the following optimization problem:

$$\min_P E(P) := \sum_{j=1}^n \left\| \frac{d\Psi}{dx}(x_j, P, \mathbf{q}) - \mathbf{f}(x_j, \Psi(x_j, P, \mathbf{q})) \right\|^2. \quad (7)$$

More details on the construction of trial solutions and the minimization problem concerning our approach are given in Section 4. In order to deal with the problem (7), one usually needs quantities such as the derivatives of $N_i(x, \mathbf{p}_i, \mathbf{q})$ with respect to the input x and the weights and biases represented by \mathbf{p}_i . They can be obtained in several ways, e.g. by computing analytical derivatives, by using finite difference or other numerical approximations, by symbolic differentiation or by automatic differentiation (see, e.g., [46] and the references therein).

Although a specialized form of automatic differentiation, known as back-propagation, is widely used in ANNs, in this work, we can easily compute analytical first-order derivatives (see also [42]), and then apply to problem (7) a variety of numerical methods that use those derivatives [40]. For a Single-Input-Single-Output (SISO) NN (i.e. $d = 1$ and $k = 1$), with n points and one hidden layer with h elements in (5), it is straightforward to show that the first-order derivative with respect to x_l , $l = 1, 2, \dots, n$, is given by

$$\frac{\partial N}{\partial x_l} = \sum_{j=1}^h w_j^o \frac{\partial \Phi_j}{\partial x_l}, \quad (8)$$

while the derivatives of the network with respect to the training parameters, which are in general the input and output weights w_j and w_j^o , $j = 1, 2, \dots, h$ are given by:

$$\frac{\partial N}{\partial w_j} = \sum_{i=1}^h w_i^o \frac{\partial \Phi_i}{w_j}, \quad \frac{\partial N}{\partial w_j^o} = \Phi_j. \quad (9)$$

(Note that we use the lightface notation N to indicate the SISO version of the neural network \mathcal{N}). Once we have the above derivatives of N , we can compute the first-order derivatives of the cost function in (7) with respect to the parameters of N , and thus we are in principle able to train the network by any minimization technique using those derivatives. However, the training phase may require a very large computing time, thus we address a strategy that optimizes the parameters via the solution of a suitable least-squares problem.

Our proposed FNN is based on radial basis transfer functions, introduced in the next section. We remark that another natural choice for the transfer function, widely used in ANN, is a sigmoidal function, which is a bounded monotone S-shaped function with a bell-shaped first derivative (see, e.g. [57]).

3.2 Radial Basis Function Neural Networks

Radial Basis Function Neural Networks (RBFNNs) are special cases of ANNs where each hidden unit is associated with a radial basis function. Powell introduced radial basis functions (RBFs) in 1985 for multivariate function interpolation ([58]). As transfer functions in ANN, RBFs were first addressed by Broomhead and Lowe ([5]). An RBF is a function $\phi_{\mathbf{c}} : \mathbb{R}^n \rightarrow \mathbb{R}$ whose value depends only on the distance between its argument \mathbf{x} and some fixed point \mathbf{c} called center:

$$\phi_{\mathbf{c}}(\mathbf{x}) = \phi(\|\mathbf{x} - \mathbf{c}\|), \quad (10)$$

where $\|\cdot\|$ denotes a vector norm.

A widely used RBF is the Gaussian RBF:

$$G(\mathbf{x}, \mathbf{c}, \sigma) = \exp\left(-\frac{\|\mathbf{x} - \mathbf{c}\|^2}{\sigma^2}\right), \quad (11)$$

employed with the Euclidean norm. A Gaussian RBF is characterized by the width or scale parameter σ .

In RBFNNs, each hidden unit is more ‘‘sensitive’’ to data points close to its center. Furthermore, for Gaussian RBFNNs, this sensitivity can be tuned by adjusting the width parameter σ : a larger σ implies less sensitivity. Thus, for most of the problems, the choice of the centers is crucial. For the specific case of RBFNNs with the same σ in all hidden nodes, Park and Sandberg proved that those networks are capable of universal approximation [56]. Furthermore, Liao et al. extended this result to very mild hypotheses on the activation function [45]. In Section 4, we suggest a choice of these parameters in the context of solving problems of ODEs.

Theorem 3.1. *Let $\phi_{\mathbf{c}}$ be as in equation (10). If $\phi_{\mathbf{c}}$ is continuous almost everywhere, locally essentially bounded, and not a polynomial, then for any compact set $K \subset \mathbb{R}^n$, $\Sigma = \text{span}\{\phi_{\mathbf{c}}(w\mathbf{x} + \mathbf{b}) : w \in \mathbb{R}, \mathbf{b} \in \mathbb{R}^n\}$ is dense in $C(K)$ with respect to the uniform norm, i.e., given any $g \in C(K)$ and $\epsilon > 0$, there exists $\gamma \in \Sigma$ such that*

$$\|\gamma - g\|_{L^\infty(K)} \leq \epsilon.$$

RBFNNs have gained popularity because of a number of advantages compared to other types of ANNs, including their simpler structure and faster learning algorithms. RBFNNs have been applied to problems in many different areas, such as image processing [20, 51, 75]), speech recognition [2, 62, 70], time series analysis [76], adaptive equalization [11, 13] and others.

3.3 Random Projection RBFNNs

The training of an ANN requires the minimization of a cost function. But, even for the simple case of SLFNNs, this task may become challenging. Many optimization algorithms used for training ANNs apply stochastic gradient-based approaches which back-propagate the error and adjust the weights through specific directions [4]. More recently, second-order stochastic optimization methods have been widely investigated to get better performances than first-order methods, especially when ill-conditioned problems must be solved (see, e.g., [66] and the references therein). Nevertheless, there are still difficulties in using these approaches, such as the setting of the so-called hyperparameters, the significant increase of computing time when the number of data or the number of nodes in the hidden layer grows, and the high non-convexity stemming from the use of nonlinear activation functions, which can lead the algorithms to local minima.

A way to deal with the ‘‘curse of dimensionality’’ in training ANNs is to apply the concept of random projection. The idea behind random projections is to construct a Lipschitz mapping that projects the data into a random subspace. The feasibility of this approach can be justified by the celebrated Johnson and Lindenstrauss (JL) Theorem: [38]:

Theorem 3.2 (Johnson and Lindenstrauss). *Let \mathcal{X} be a set of n points in \mathbb{R}^d . Then, $\forall \epsilon \in (0, 1)$ and $k \in \mathbb{N}$ such that $k \geq O(\frac{\ln n}{\epsilon^2})$, there exists a map $\mathbf{F} : \mathbb{R}^d \rightarrow \mathbb{R}^k$ such that*

$$(1 - \epsilon)\|\mathbf{u} - \mathbf{v}\|^2 \leq \|\mathbf{F}(\mathbf{u}) - \mathbf{F}(\mathbf{v})\|^2 \leq (1 + \epsilon)\|\mathbf{u} - \mathbf{v}\|^2 \quad \forall \mathbf{u}, \mathbf{v} \in \mathcal{X}. \quad (12)$$

Note that while the above theorem is deterministic, its proof relies on probabilistic techniques combined with Kirschbraun’s theorem to yield a so-called extension mapping [38]. In particular, it can be shown that one of the many such embedding maps is simply a linear projection matrix with suitable random entries. Then, the JL Theorem may be proved using the following lemma.

Lemma 3.1. *Let \mathcal{X} be a set of n points in \mathbb{R}^d and let $\mathbf{F}(\mathbf{u})$ be the random projection defined by*

$$\mathbf{F}(\mathbf{u}) = \frac{1}{\sqrt{k}} R \mathbf{u}, \quad \mathbf{u} \in \mathbb{R}^d,$$

where $R = [r_{ij}] \in \mathbb{R}^{k \times d}$ has components that are i.i.d. random variables sampled from a normal distribution. Then, $\forall \mathbf{u} \in \mathcal{X}$

$$(1 - \epsilon) \|\mathbf{u}\|^2 \leq \|\mathbf{F}(\mathbf{u})\|^2 \leq (1 + \epsilon) \|\mathbf{u}\|^2$$

is true with probability $p \geq 1 - 2 \exp(-(\epsilon^2 - \epsilon^3) \frac{k}{4})$.

Similar proofs have been given for distributions different from the normal one (see, e.g., [1, 15, 69, 72]). In general, the proof of the JL Theorem is based on the fact that inequality (12) is true with probability 1 if k is large enough. Thus, the theorem states that there exists a projection (referred to as encoder) of \mathcal{X} into a random subspace of dimension $k \geq O(\frac{\ln n}{\epsilon^2})$, where the distance between any pair of points in the embedded space $F(\mathcal{X})$ is bounded in the interval $[1 - \epsilon, 1 + \epsilon]$. Moreover, [15] proved that if the random projection is of Gaussian type, then a lower bound of the embedding dimension is given by $k \geq 4(\epsilon^2/2 - \epsilon^3/3)^{-1} \ln n$.

We note that the above mapping is a feature mapping, which in principle may result in a dimensionality reduction ($k < d$) or a projection into a higher dimensional space ($k > d$) in which one seeks a linear low-dimensional manifold (in analogy to the case of kernel-based manifold learning methods). We also note that while the above linear random projection is but one of the choices for constructing a JL embedding (and proving it), it has been experimentally demonstrated and/or theoretically proven that appropriately constructed nonlinear random embeddings may outperform simple linear random projections. For example, in [25] it was shown that deep networks with random weights for each layer result in even better approximation accuracy than the simple linear random projection. Based on the concept of random projection, Schmidt et al. [65] performed computational experiments using FNNs with sigmoidal transfer functions in the hidden layer and a bias on the output layer, thus showing that by fixing the weights between the input and the hidden layer at random values, and by training the output weights via the solution of linear equations stemming from the Fisher minimization problem, the approximation accuracy is equivalent to that obtained with the standard back-propagation iterative procedure where all the weights are calibrated.

In the same year, Random Vector Functional-Link Networks (RVFLNs) were addressed in [54], in which the input layer is directly connected also to the output layer, the internal weights are chosen randomly in $[-1, 1]$ and the output weights are estimated in one step by solving a system of linear equations. By formulating a limit-integral of the function to be approximated with Monte Carlo simulations, in [35], it was proved that RVFLNs are universal approximators for continuous functions on bounded finite-dimensional sets and that the rate at which the approximation error vanishes is of the order of $\frac{1}{n}$, where n is the number of basis functions parametrized by random variables. Extensive computational experiments performed in [77] showed that the direct links employed in RVFLNs between the input and the output layer play an important role for the performance, while the bias of the output neuron is not so important.

Reservoir Computing (otherwise called Eco State Networks) is another approach to network training based on the concept of random projection [8, 36, 48, 71]. The basic structure of Reservoir Computing consists of a Recurrent Neural Network (RNN) with a large number of hidden units, an extra input and an extra output unit. Internal connection weights form a sparse random connectivity pattern with fixed values. The estimation of the optimal output weights is achieved by solving a system of linear equations arising from a mean-squares minimization problem.

Furthermore, it has been shown that single-layer FNNs with randomly assigned input weights and biases of the hidden layer, and with infinitely differentiable functions at the hidden layer called Extreme Learning Machines (ELMs) can universally approximate any continuous function on any compact input set [29, 30, 31, 33]. For the case of a FNN with a single hidden layer of h units, the random projection of the input space can be written as

$$Y = \Phi(X), \tag{13}$$

where the columns of the matrix $X \in \mathbb{R}^{d \times n}$ represent a set of n points in the input d -dimensional space, the columns of $Y \in \mathbb{R}^{k \times n}$ are the corresponding random projections, and $\Phi : \mathbb{R}^{d \times n} \rightarrow \mathbb{R}^{k \times n}$ acts as an encoder, i.e. a family of transfer functions whose parameters are sampled from a certain random distribution function. If the values of the weights w_{ij} between the input and the hidden layer are fixed, then $\forall \mathbf{x} \in \mathbb{R}^d$ the random projection can be written as a linear map:

$$Y = W^o \Phi, \quad Y \in \mathbb{R}^{k \times n}, \tag{14}$$

where $\Phi \in \mathbb{R}^{h \times n}$ is a random matrix containing the outputs of the nodes of the hidden layer as shaped by the h random distribution functions (e.g., RBFs or sigmoidal functions) and the d -dimensional inputs. Thus, the so-called ELMs can be seen as underdetermined linear systems in which the output weights are estimated by solving minimum-norm least-squares problems [3, 30, 31, 33]. Moreover, for ELMs an interpolation-like theorem has been proven by Huang et al. in [33]:

Theorem 3.3. *Let us consider a single-hidden-layer FNN with h hidden units and an infinitely differentiable transfer function $\phi : \mathbb{R} \rightarrow \mathbb{R}$, n distinct input-output pairs $(\mathbf{x}_i, \mathbf{y}_i) \in \mathbb{R}^d \times \mathbb{R}^k$, and randomly chosen values from any continuous probability distribution for the internal weights w_{ij} and for the values of the biases of the h neurons of the hidden layer, grouped in $\mathbf{b} \in \mathbb{R}^h$. Let us also denote by $W \in \mathbb{R}^{h \times d}$ and $W^o \in \mathbb{R}^{k \times h}$ the matrices containing the internal and output weights, and by $X \in \mathbb{R}^{d \times n}$ and $Y \in \mathbb{R}^{k \times n}$ the matrices with columns \mathbf{x}_i and \mathbf{y}_i . Then, the hidden layer output matrix $\Phi \in \mathbb{R}^{h \times n}$, whose elements are determined by the action of the transfer functions on $WX + \mathbf{b}\mathbf{1}^T$ (where $\mathbf{1} \in \mathbb{R}^n$ has all the entries equal to 1), has full rank and*

$$\|W^o\Phi - Y\| = 0$$

with probability 1.

A review on neural networks with random weights can be found in [10].

4 The Proposed Method

Here, we focus on the numerical solution of the initial-value problem (1) in an interval $[x_0, x_{end}]$. Based on the previous notation, for this problem $d = 1$ and $k = m$. Thus, we denote by $\Psi_i(x, \mathbf{w}_i^o, \mathbf{p}_i)$ the i th component of the trial solution $\Psi(x, W^o, P)$ defined in (6), where $W^o \in \mathbb{R}^{m \times h}$ is the matrix containing the weights w_{ij}^o between the hidden and the output layer. Note that we separate W^o from the other network parameters consisting of the input weights, the biases of the hidden layer and the parameters of the transfer function, and denote those parameters again by P , with a little abuse of notation. Furthermore, the vector of hyperparameters \mathbf{q} in (6) is neglected because we do not use it. Following [42] and taking into account that the trial solution must satisfy the initial value conditions $y_i(x_0) = \alpha_i$, $i = 1, 2, \dots, m$, we set:

$$\Psi_i(x, \mathbf{w}_i^o, \mathbf{p}_i) = \alpha_i + (x - x_0)N_i(x, \mathbf{w}_i^o, \mathbf{p}_i), \quad (15)$$

where $N_i(x, \mathbf{w}_i^o, \mathbf{p}_i)$ is a single-output FNN with parameters the output weights $\mathbf{w}_i^o = [w_{1i}^o \ w_{2i}^o \ \dots \ w_{hi}^o]^T \in \mathbb{R}^h$, and \mathbf{p}_i contains the remaining parameters associated with that network. Then, if one considers the numerical solution based on n collocation points x_1, x_2, \dots, x_n , the error function we seek to minimize for training the FNN is given by:

$$E(W^o, P) = \sum_{i=1}^m \sum_{j=1}^n \left(\frac{d\Psi_i}{dx}(x_j, \mathbf{w}_i^o, \mathbf{p}_i) - f_i(x_j, \Psi_1(x_j, \mathbf{w}_1^o, \mathbf{p}_1), \dots, \Psi_m(x_j, \mathbf{w}_m^o, \mathbf{p}_m)) \right)^2. \quad (16)$$

Here, we propose a RPNN for the solution of ODEs that has n input collocation points, h nodes in the hidden layer with Gaussian RBFs, and m single-input-single output neural sub-networks with a linear output transfer function. In particular, we consider each sub-network N_i to be a linear combination of RBFs, as specified next:

$$N_i(x, \mathbf{w}_i^o, \mathbf{p}_i) = \sum_{j=1}^h w_{ji}^o G_{ji}(x), \quad i = 1, 2, \dots, m, \quad (17)$$

where

$$G_{ji}(x) = G(w_{ji}x + b_{ji}, c_j, \sigma_{ji}) = \exp\left(-\frac{(w_{ji}x + b_{ji} - c_j)^2}{\sigma_{ji}}\right), \quad (18)$$

$$j = 1, 2, \dots, h, \quad i = 1, 2, \dots, m,$$

with $w_{ji} = 1$ and $c_j = x_0 + (j - 1)\bar{s}$ with $\bar{s} = (x_{end} - x_0)/(h - 1)$ and $j = 1, \dots, h$. Notice that in the above configuration, we fix all the internal weights to 1 and the centers to be equidistant in the domain, while we set randomly from appropriately chosen uniform distributions the biases b_{ji} and the width parameters σ_{ji} . This configuration is slightly different from the classical ELM configuration with RBFs, where the internal weights are set equal to 1 and the biases equal to 0, while the centers are randomly uniformly distributed in $[-1, 1]$ (see, e.g., [32]). However, it is straightforward to show that we still get universal approximation properties, as stated in the next theorem.

Theorem 4.1. *Let us fix a continuous (target) function φ and consider the system of functions $\{N_i(x, \mathbf{w}_i^o, \mathbf{p}_i)\}_{i=1, \dots, m}$ in (17), with G_{ji} , w_{ji} and c_j defined in (18) and the subsequent lines. Then, for every sequence of randomly chosen parameters \mathbf{p}_i there exists a choice of \mathbf{w}_i^o such that*

$$\lim_{m \rightarrow \infty} \|N_i(x, \mathbf{w}_i^o, \mathbf{p}_i) - \varphi(x)\| = 0 \text{ with probability one.}$$

Proof. Since w_{ji} and c_j are fixed, one can manipulate (18) and write it as

$$G_{ji}(x) = \exp\left(-\frac{(x + \alpha_{ji})^2}{\beta_{ji}}\right),$$

where the parameters $\alpha_{ji} = b_{ji} - c_j$ and $\beta_{ji} = \sigma_{ji}$ are random variables (because b_{ji} and σ_{ji} are random variables sampled from continuous probability distributions). Therefore, the network fits the hypotheses of an FNN with random hidden nodes. Because the considered RBFs are sufficiently regular, Theorem II.1 in [32] holds and hence the thesis follows in a straightforward manner. \square

Under the previous assumptions, the derivative of the i th component Ψ_i of the trial solution with respect to the collocation point x_l is given by (see (8)):

$$\frac{\partial \Psi_i}{\partial x_l} = N_i(x_l, \mathbf{w}_i^o, \mathbf{p}_i) - (x_l - x_0) \sum_{j=1}^h \frac{2}{\sigma_{ji}} w_{ji}^o (x_l + b_{ji} - c_j) \exp\left(-\frac{(x_l + b_{ji} - c_j)^2}{\sigma_{ji}}\right), \quad (19)$$

while, for any fixed x_l , the derivative of Ψ_i with respect to the only unknown parameter w_{ji}^o is given by (see (15) and (9)):

$$\frac{\partial \Psi_i}{\partial w_{ji}^o} = (x_l - x_0) \exp\left(-\frac{(x_l + b_{ji} - c_j)^2}{\sigma_{ji}}\right). \quad (20)$$

For the determination of the randomized parameters of the Gaussian RBF, we need to fix reference intervals where to look for these parameters. Our requests are that the functions are neither too steep nor too flat in the reference interval, and on each collocation point there are at least two basis functions giving values that are not too small. Then, based on numerical experiments, the biases b_{ji} of the hidden units and the parameters σ_{ji} are taken to be uniformly randomly distributed in the intervals

$$\left[-\frac{(x_{end} - x_0)}{6} - \bar{s}, -\bar{s}\right] \text{ and } \left[\frac{1}{10}, \frac{20(x_{end} - x_0)}{3}\right],$$

respectively. We emphasise that this choice appears to be problem independent. Therefore, the only parameters that have to be determined by training the network are the output weights w_{ji}^o . Hence, for the n collocation points x_l , the outputs of each network N_i , $i = 1, 2, \dots, m$, are given by:

$$\mathbf{N}_i(x_1, x_2, \dots, x_n, \mathbf{w}_i^o, \mathbf{p}_i) = \mathbf{R}_i \mathbf{w}_i^o, \quad (21)$$

where $\mathbf{N}_i(x_1, x_2, \dots, x_n, \mathbf{w}_i^o, \mathbf{p}_i) \in \mathbb{R}^n$ is the vector with l th component the output of N_i corresponding to x_l , and $\mathbf{R}_i = \mathbf{R}_i(x_1, \dots, x_n, \mathbf{p}_i) \in \mathbb{R}^{n \times h}$ is defined as

$$\mathbf{R}_i(x_1, \dots, x_n, \mathbf{p}_i) = \begin{bmatrix} G_{1i}(x_1) & \cdots & G_{hi}(x_1) \\ \vdots & \vdots & \vdots \\ G_{1i}(x_n) & \cdots & G_{hi}(x_n) \end{bmatrix}. \quad (22)$$

The minimization of the error function given in (16) is achieved by a Gauss-Newton scheme (see, e.g., [40]) over nm nonlinear residuals F_q , with $q = l + (i - 1)n$, $i = 1, 2, \dots, m$, $l = 1, 2, \dots, n$, given by:

$$F_q(W^o) = \frac{d\Psi_i}{dx_l}(x_l, \mathbf{w}_i^o, \mathbf{p}_i) - f_i(x_l, \Psi_1(x_l, \mathbf{w}_1^o, \mathbf{p}_1), \dots, \Psi_m(x_l, \mathbf{w}_m^o, \mathbf{p}_m)). \quad (23)$$

By setting $\mathbf{F}(W^o) = [F_1(W^o) \cdots F_{nm}(W^o)]^T$ and looking at W^o as a vector where the m unknown output weights \mathbf{w}_i^o are stacked, i.e.

$$W^o = \begin{bmatrix} \mathbf{w}_1^o \\ \mathbf{w}_2^o \\ \vdots \\ \mathbf{w}_m^o \end{bmatrix} \in \mathbb{R}^{mh},$$

the Gauss-Newton method reads:

$$W^{o(\nu+1)} = W^{o(\nu)} + dW^{o(\nu)}, \quad dW^{o(\nu)} = \arg \min_{W^o} \|(\nabla_{W^o} \mathbf{F}(W^{o(\nu)}))^T dW + \mathbf{F}(W^{o(\nu)})\|, \quad (24)$$

where (ν) denotes the current iteration and $\nabla_{W^o} \mathbf{F} \in \mathbb{R}^{nm \times mh}$ is the Jacobian matrix of \mathbf{F} with respect to W^0 :

$$\nabla_{W^o} \mathbf{F}(W^{o(\nu)}) = \begin{bmatrix} \frac{\partial F_1}{\partial w_{11}^o} & \frac{\partial F_1}{\partial w_{12}^o} & \cdots & \frac{\partial F_1}{\partial w_{1h}^o} & \cdots & \frac{\partial F_1}{\partial w_{1(mh)}^o} \\ \frac{\partial F_2}{\partial w_{11}^o} & \frac{\partial F_2}{\partial w_{12}^o} & \cdots & \frac{\partial F_2}{\partial w_{1h}^o} & \cdots & \frac{\partial F_2}{\partial w_{1(mh)}^o} \\ \vdots & \vdots & \ddots & \vdots & \ddots & \vdots \\ \frac{\partial F_q}{\partial w_{11}^o} & \frac{\partial F_q}{\partial w_{12}^o} & \cdots & \frac{\partial F_q}{\partial w_{1h}^o} & \cdots & \frac{\partial F_q}{\partial w_{1(mh)}^o} \\ \vdots & \vdots & \ddots & \vdots & \ddots & \vdots \\ \frac{\partial F_{nm}}{\partial w_{11}^o} & \frac{\partial F_{nm}}{\partial w_{12}^o} & \cdots & \frac{\partial F_{nm}}{\partial w_{1h}^o} & \cdots & \frac{\partial F_{nm}}{\partial w_{1(mh)}^o} \end{bmatrix} \Big|_{(W^{o(\nu)})}. \quad (25)$$

Note that the residuals depend on the derivatives $\frac{\partial \Psi_i}{\partial x_l}$ in (19) and the trial functions Ψ_i in (15), while the elements of the Jacobian matrix depend on the derivatives of $\frac{\partial \Psi_i}{\partial w_{ji}^o}$ in (20) as well as on the mixed derivatives $\frac{\partial^2 \Psi_i}{\partial x_l \partial w_{ji}^o}$, which, based on (19), are given by

$$\frac{\partial^2 \Psi_i}{\partial x_l \partial w_{ji}^o} = \frac{\partial N_i(x_l, \mathbf{w}_i^o, \mathbf{p}_i)}{\partial w_{ji}^o} - (x_l - x_0) \frac{2}{\sigma_{ji}} (x_l + b_{ji} - c_j) \exp\left(-\frac{(x_l + b_{ji} - c_j)^2}{\sigma_{ji}}\right), \quad (26)$$

where

$$\frac{\partial N_i(x_l, \mathbf{w}_i^o, \mathbf{p}_i)}{\partial w_{ji}^o} = \exp\left(-\frac{(x_l + b_{ji} - c_j)^2}{\sigma_{ji}}\right). \quad (27)$$

As in general $h > n$, the minimization problem in (24) is an underdetermined linear system, and we compute its solution requiring a minimum L_2 norm. This can be performed by using the Moore-Penrose pseudoinverse of the Jacobian matrix with the Singular Value Decomposition. More precisely, we estimate the pseudoinverse by cutting off all the singular values (and their corresponding singular vectors) below a small tolerance ϵ . This allows us to deal with the case where the Jacobian is rank deficient, which may happen because the RBFs are not injective functions. Furthermore, this choice also allows us to cope with the difference between the exact rank and the numerical rank of the Jacobian matrix. Following [26], for some small ϵ the ϵ -rank of a matrix $M \in \mathbb{R}^{mn \times mh}$ is defined as follows:

$$r_\epsilon = \min\{\text{rank}(B) \in \mathbb{R}^{mn \times mh} : \|M - B\|_{L_2} \leq \epsilon\}. \quad (28)$$

Then, if ϵ is ‘‘small enough’’, we neglect all the singular values below ϵ and approximate the pseudoinverse of the Jacobian matrix as

$$(\nabla_{W^o} \mathbf{F})^+ = V_{r_\epsilon} \Sigma_{r_\epsilon}^+ U_{r_\epsilon}^T, \quad (29)$$

where $\Sigma_{r_\epsilon} \in \mathbb{R}^{r_\epsilon \times r_\epsilon}$ is the diagonal matrix with the r_ϵ largest singular values of $\nabla_{W^o} \mathbf{F}$, $\Sigma_{r_\epsilon}^+$ is its pseudoinverse, and $U_{r_\epsilon} \in \mathbb{R}^{mn \times r_\epsilon}$ and $V_{r_\epsilon} \in \mathbb{R}^{mh \times r_\epsilon}$ are the matrices with columns the corresponding r_ϵ left and right eigenvectors, respectively. The value of ϵ used in our experiments is specified at the beginning of Section 5. Thus, the direction $dW^{o(\nu)}$ at each Gauss-Newton iteration is given by

$$dW^{o(\nu)} = -V_{r_\epsilon} \Sigma_{r_\epsilon}^+ U_{r_\epsilon}^T \mathbf{F}(W^{o(\nu)}).$$

We can summarize the proposed method in the pseudo-code shown in Algorithm 1, where $\mathcal{U}(a, b)$ denotes the uniform random distribution in the interval $[a, b]$ and tol is a tolerance used in the Gauss-Newton stopping criterion.

5 Numerical results

We implemented the Algorithm 1 using MATLAB 2021a on an Intel Core i5-8265U with up to 3.9 GHz frequency and a memory of 8 GB. The Moore-Penrose pseudoinverse of $\nabla_{w^o} \mathbf{F}$ was computed with the MATLAB built-in function `pinv`, with a singular value tolerance $\epsilon = 10^{-4}$. For our simulations, we chose two well-known and challenging stiff ODE systems: the ROBER and the van der Pol system (the latter becomes stiff as its parameter μ increases). For comparison purposes, we also solved the ODE problems with two widely used MATLAB built-in functions, namely `ode45`, implementing an adaptive-step Runge-Kutta method based on the Dormand-Prince pair, and `ode15s`, implementing a variable-step variable-order multistep method based on numerical differentiation formulas. In order to estimate the

Algorithm 1: solving ODE systems using a RPNN with RBF functions**DATA: ODE problem and grid points**

$\frac{dy_i}{dx} = f_i(x, y_1, y_2, \dots, y_m)$ in $[x_0, x_{end}]$, $y_i(x_0) = \alpha_i$, $i = 1, 2, \dots, m$
 $x_j \in [x_0, x_{end}]$, $j = 1, \dots, n$, distinct points

STEP 1: choose trial solution

$\Psi_i(x, \mathbf{w}_i^0, \mathbf{p}_i) = \alpha_i + (x - x_0)N_i(x, \mathbf{w}_i^0, \mathbf{p}_i)$, $i = 1, \dots, m$, $N_i(x, \mathbf{w}_i^0, \mathbf{p}_i)$ defined in (17) with $w_{ji} = 1$

STEP 2: fix some parameters and weights

$\bar{s} \leftarrow \frac{x_{end} - x_0}{h - 1}$
 $c_j \leftarrow x_0 + j\bar{s}$, $j = 1, \dots, h$
 $b_{ji} \sim \mathcal{U}\left(-\frac{x_{end} - x_0}{6} - \bar{s}, -\bar{s}\right)$, $j = 1, \dots, h$, $i = 1, \dots, m$
 $\sigma_{ji} \sim \mathcal{U}\left(\frac{1}{10}, \frac{20(x_{end} - x_0)}{3}\right)$, $j = 1, \dots, h$, $i = 1, \dots, m$

STEP 3: compute W^0 **repeat**

for $j = 1, \dots, n$, $i = 1, \dots, m$ **do**

$q = j + (i - 1)n$

$F_q(W^o) \leftarrow \frac{d\Psi_i}{dx}(x_l, \mathbf{w}_i^o, \mathbf{p}_i) - f_i(x_l, \Psi_1(x_l, \mathbf{w}_1^o, \mathbf{p}_1), \Psi_2(x_l, \mathbf{w}_2^o, \mathbf{p}_2), \dots, \Psi_m(x_l, \mathbf{w}_m^o, \mathbf{p}_m))$ (see (23))

end

set $\mathbf{F}(W^o) = [F_1(W^o) F_2(W^o) \dots F_{nm}(W^o)]^T$ and compute $\nabla_{W^o} \mathbf{F}(W^o)$

apply SVD to find the pseudo-inverse: $(\nabla_{W^o} \mathbf{F})^+ = V_{r_e} \Sigma_{r_e}^+ U_{r_e}^T$,

update the unknown weights: $W^o \leftarrow W^o - (\nabla_{W^o} \mathbf{F}(W^o))^+ \mathbf{F}(W^o)$

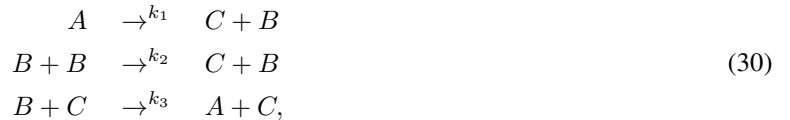
$err \leftarrow \|(\nabla_{W^o} \mathbf{F}(W^o))^+ \mathbf{F}(W^o)\|$

until $err < tol$;

error in the solution computed with our RPNN approach, we used as reference solution the one computed by ode15s with absolute and relative error tolerances equal to 10^{-8} . To this aim, we computed the L_2 and the L_∞ norms of the differences between the computed and the reference solutions, as well as the Mean Absolute Error (MAE); all the above performance metrics are being evaluated at the n grid collocation points where the solution is sought with the proposed RPNN algorithm. Finally, we ran each solver 100 times and computed the median, 5th percentile and 95th percentile of the execution time, in seconds. The time of each run was measured by using the MATLAB commands `tic` and `toc`. Henceforth, we use t instead of x , since the independent variable in the test problems represents time. We also assume $t_0 = x_0 = 0$.

5.1 Case study 1: ROBER system

The ROBER model was developed by Robertson to describe the kinetics of an autocatalytic reaction [63]. The set of the reactions reads:



where A, B, C are chemical species and k_1 , k_2 and k_3 are reaction rate constants. Assuming idealized conditions and that the mass action law is applied for the rate functions, we have the following system of ODEs:

$$\begin{aligned} y_1' &= -k_1 y_1 + k_3 y_2 y_3 \\ y_2' &= k_1 y_1 - k_2 y_2^2 - k_3 y_2 y_3 \\ y_3' &= k_2 y_2^2, \end{aligned} \quad (31)$$

where y_1 , y_2 and y_3 denote the concentrations of A, B and C, respectively. The ROBER problem has been used as a benchmark problem to test stiff ODE integrators.

In our simulations, we set the typical values of the parameters, i.e. $k_1 = 0.04$, $k_2 = 3 \times 10^3$ and $k_3 = 10$, and $y_1(0) = 1$, $y_2(0) = 0$ and $y_3(0) = 0$ as initial values of the concentrations. Stiffness arises from the large difference among the reaction rate constants. Based on the proposed methodology, we construct three trial solutions:

$$\begin{aligned}\Psi_1(t) &= \alpha_1 + tN_1(t, \mathbf{w}_1^o), \\ \Psi_2(t) &= \alpha_2 + tN_2(t, \mathbf{w}_2^o), \\ \Psi_3(t) &= \alpha_3 + tN_3(t, \mathbf{w}_3^o),\end{aligned}$$

where $\alpha_1 = 1$, $\alpha_2 = 0$ and $\alpha_3 = 0$ and the p_i 's have been neglected because they have been fixed. The error function to be minimized is given by:

$$\begin{aligned}E(\mathbf{w}_1^o, \mathbf{w}_2^o, \mathbf{w}_3^o) &= \sum_{i=1}^n \left(\left(\frac{d\Psi_1}{dt}(t_i, \mathbf{w}_1^o) - f_1(t_i, \Psi_1, \Psi_2, \Psi_3) \right)^2 \right. \\ &\quad + \left(\frac{d\Psi_2}{dt}(t_i, \mathbf{w}_2^o) - f_2(t_i, \Psi_1, \Psi_2, \Psi_3) \right)^2 \\ &\quad \left. + \left(\frac{d\Psi_3}{dt}(t_i, \mathbf{w}_3^o) - f_3(t_i, \Psi_1, \Psi_2, \Psi_3) \right)^2 \right),\end{aligned}$$

where

$$\begin{aligned}f_1 &= -k_1(\alpha_1 + t_i N_1(t_i, \mathbf{w}_1^o)), \\ f_2 &= k_1(\alpha_1 + t_i N_1(t_i, \mathbf{w}_1^o)) - k_2 t_i^2 N_2(t_i, \mathbf{w}_2^o)^2 - k_3 t_i^2 N_2(t_i, \mathbf{w}_2^o) N_3(t_i, \mathbf{w}_3^o), \\ f_3 &= k_2 t_i^2 N_2(t_i, \mathbf{w}_2^o)^2.\end{aligned}$$

For the numerical solution of the ROBER system with the proposed method, we used a grid of $n = 14$ equidistant collocation points in the time interval $[0, 1.8]$. We also set $h = 144$ and hence $\bar{s} \simeq 0.0126$. For our illustrations, we tested the numerical performance of the scheme using two values of the tolerance tol , i.e. 10^{-2} and 10^{-3} . For comparison purposes, we used the same values of both the absolute and relative error tolerances for the functions `ode45` and `ode15s`. The approximate solutions obtained with tolerances 10^{-2} and 10^{-3} are shown in Figure 1. Furthermore, in Tables 1 and 2, we report the corresponding numerical approximation accuracy obtained with the various methods in terms of the MAE, L_2 -norm and L_∞ -norm of the error with respect to the reference solution. Here, in order to compute these errors, we evaluated the corresponding solutions in the grid points t_i . In Table 3, we show the number of points required by each method, and in Table 4, we report the execution times (median, 5th percentile and 95th percentile) of all the methods, including the time required to compute the reference solution. Finally, in Tables 5 and 6, we present the errors of the approximate solutions obtained with both tolerances, evaluated at 1000 equidistant points in $[0, 1.8]$. We note that for `ode45` and `ode15s` the values of the solutions at these points were obtained by using the MATLAB function `deval`, which uses an interpolation technique.

As it is shown, with tolerances equal to 10^{-2} the proposed machine learning method achieves more accurate solutions than `ode15s`, while `ode45` fails to converge (see Tables 1,5). The number of points used by our approach is smaller than or equal to those used by the other two methods (see Table 3). On the other hand, the computing time of our method is larger (Table 4), but we believe this is paid off by the fact that our method does not require the user to explicitly take into account the stiffness of the ODE problem and it provides an approximate solution in the form of a function that can be evaluated at points different from the collocation ones. The good approximation properties of this function is confirmed by the errors in the solutions evaluated at the 1000 points, which show that the proposed RPNN approach outperforms the `ode15s` for all metrics (see Table 5). Finally, we believe that the code implementing the proposed scheme can be made more efficient, but this is beyond the scope of the current work.

When the tolerances are set equal to 10^{-3} , the proposed method provides a solution whose error is generally comparable or slightly worse than the errors in the solutions computed by the other two methods, in both cases where the solution is evaluated at the points t_i and at the additional 1000 points. We also note that `ode45` is now able to compute an approximate solution to the problem. The execution time required by the RPNN method is again larger than the times of the classical methods, but the comments made for the case of the tolerances equal to 10^{-2} still apply.

5.2 Case study 2: van der Pol system

The van der Pol model is given by the following equations:

$$y_1'' - \mu(1 - y_1^2)y_1' + y_1 = 0, \quad (32)$$

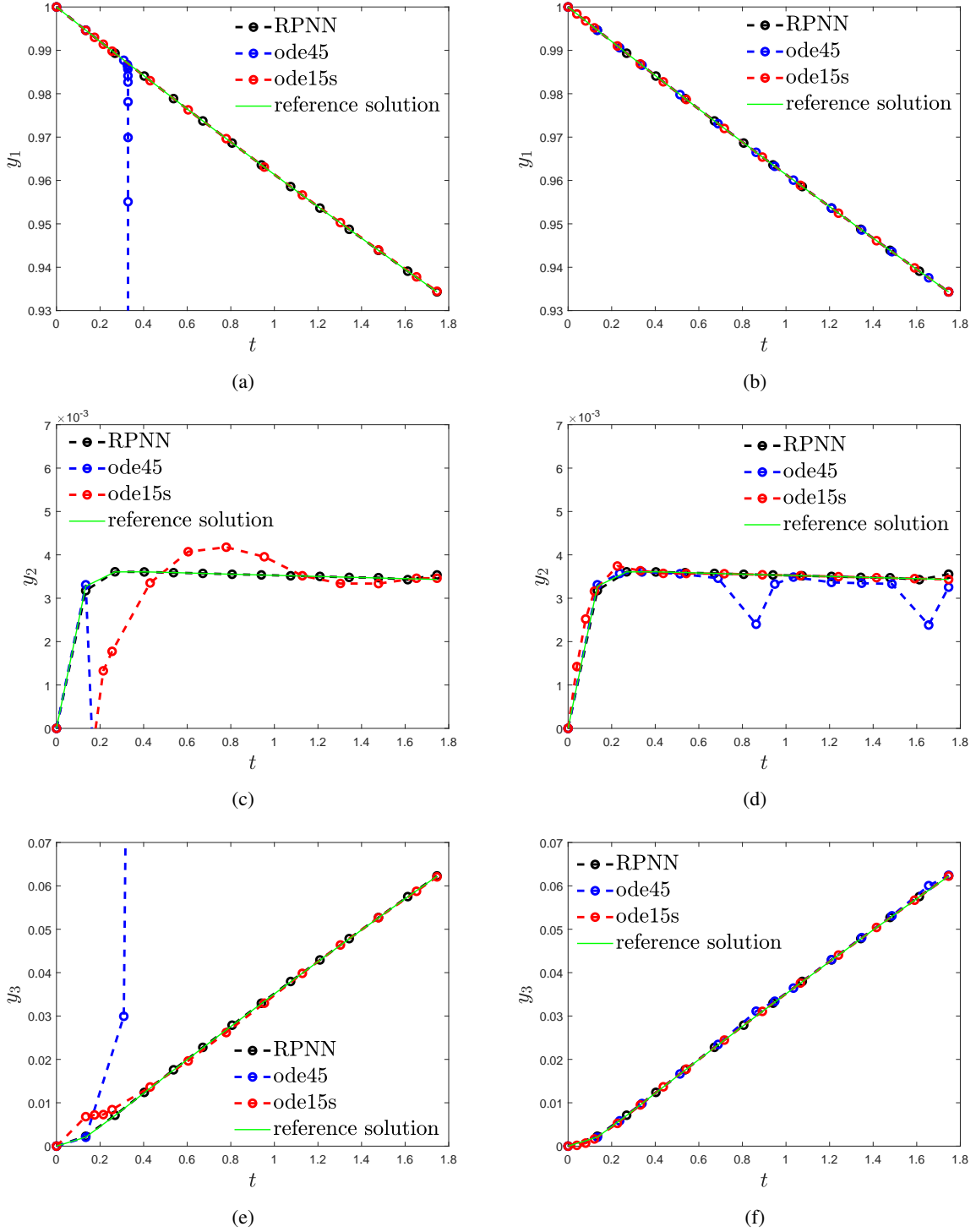


Figure 1: ROBER problem. Approximate solutions computed by the different methods in the interval $[0, 1.8]$ with tolerances set to 10^{-2} ((a), (c) and (e)) and 10^{-3} ((b), (d) and (f)).

where $\mu > 0$ is a scalar parameter. Large values of μ render the equation stiff. By setting $y'_1 = y_2$, we obtain the first-order ODE system

$$\begin{aligned} y'_1 &= y_2, \\ y'_2 &= \mu(1 - y_1^2)y_2 - y_1. \end{aligned} \quad (33)$$

Table 1: ROBER problem: L_2 -norm, L_∞ -norm and MAE of the errors between the solutions computed with tolerances set to 10^{-2} and the reference solution obtained with ode15s with tolerances set to 10^{-8} .

	y_1			y_2			y_3		
	L_2	L_∞	MAE	L_2	L_∞	MAE	L_2	L_∞	MAE
RPNN	3.27e-5	3.035e-5	4.64e-6	0.0001	0.0001	1.81e-5	0.0004	0.0002	8.86e-5
ode45	—	—	—	—	—	—	—	—	—
ode15s	0.0003	0.0001	5.24e-5	0.0051	0.0047	0.0007	0.0052	0.0047	0.0007

Table 2: ROBER problem: L_2 -norm, L_∞ -norm and MAE of the errors between the solutions computed with tolerances set to 10^{-3} and the reference solution obtained with ode15s with tolerances set to 10^{-8} .

	y_1			y_2			y_3		
	L_2	L_∞	MAE	L_2	L_∞	MAE	L_2	L_∞	MAE
RPNN	8.97e-6	6.91e-6	2.22e-6	0.0010	0.0010	0.0002	0.0006	0.0003	0.0002
ode45	7.21e-7	4.19e-7	2.10e-7	9.89e-5	9.82e-5	1.62e-5	9.89e-5	9.82e-5	1.63e-5
ode15s	6.25e-5	4.07e-5	1.62e-5	0.0002	0.0001	3.40e-5	0.0002	0.0001	5.09e-5

Table 3: ROBER problem. Number of points required in the interval $[0, 1.8]$ by ode45 and ode15s with tolerances 10^{-2} and 10^{-3} . The number of points used in the RPNN method were fixed to 14. The reference solution was computed by ode15s with tolerances equal to 10^{-8} . Note that for tolerances 10^{-2} the ode45 fails to converge even if it increases the points up to 69. In this case the matlab reports the following: Warning: Failure at t=1.172548e+00. Unable to meet integration tolerances without reducing the step size below the smallest value allowed (3.552714e-15) at time t".

	$tol = 10^{-2}$	$tol = 10^{-3}$
	# points	# points
RPNN	14	14
ode45	69	14
ode15s	14	15
reference solution	81	81

Table 4: ROBER problem. Median, 5th and 95th percentiles of computational time (in seconds) for the different methods with tolerances 10^{-2} and 10^{-3} . The reference solution was computed by ode15s with tolerances equal to 10^{-8} . ode45 fails to converge with tolerances 10^{-2} .

	10^{-2}			10^{-3}		
	median	5th perc	95th perc	median	5th perc	95th perc
RPNN	0.0224	0.0145	0.7187	0.6697	0.0420	2.2411
ode15s	0.0047	0.0034	0.0065	0.0033	0.0024	0.0056
ode45	—	—	—	9.70e-4	7.21e-4	0.0024
reference solution	0.0053	0.0038	0.0082	0.0053	0.0038	0.0082

Table 5: ROBER problem. L_2 -norm, L_∞ -norm and MAE of the errors, between the solutions computed with tolerances set to 10^{-2} and the reference solution obtained with ode15s with tolerances set to 10^{-8} , evaluated at 1000 equidistant points in $[0, 1.8]$.

	y_1			y_2			y_3		
	L_2	L_∞	MAE	L_2	L_∞	MAE	L_2	L_∞	MAE
RPNN	1.01e-4	1.75e-5	2.20e-6	0.0014	1.81e-4	1.82e-5	0.0028	2.54e-4	8.05e-5
ode45	—	—	—	—	—	—	—	—	—
ode15s	0.0021	1.33e-4	5.17e-5	0.0404	0.0046	7.06e-4	0.0409	0.0047	7.12e-4

Table 6: ROBER problem. L_2 -norm, L_∞ -norm and MAE of the errors, between the solutions computed with tolerances set to 10^{-3} and the reference solution obtained with ode15s with tolerances set to 10^{-8} , evaluated at 1000 equidistant points in $[0, 1.8]$.

	y_1			y_2			y_3		
	L_2	L_∞	MAE	L_2	L_∞	MAE	L_2	L_∞	MAE
RPNN	6.37e-4	2.01e-4	1.08e-5	0.0426	0.0096	3.64e-4	0.0315	0.0072	3.84e-4
ode45	2.36e-4	2.25e-5	5.18e-6	0.0119	0.0012	2.16e-4	0.0118	0.0012	2.15e-4
ode15s	4.57e-4	1.81e-5	1.33e-5	0.0020	2.53e-4	2.90e-5	0.0021	2.58e-4	4.18e-5

As initial conditions we consider $y_1(0) = 2$ and $y_2(0) = 0$.

We define two trial solutions:

$$\begin{aligned}\Psi_1(t) &= \alpha_1 + tN_1(t, \mathbf{w}_1^o), \\ \Psi_2(t) &= \alpha_2 + tN_2(t, \mathbf{w}_2^o),\end{aligned}\tag{34}$$

where $\alpha_1 = 2$ and $\alpha_2 = 0$. The error to be minimized is given by

$$E(\mathbf{w}_1^o, \mathbf{w}_2^o) = \sum_{i=1}^n \left(\left(\frac{d\Psi_1}{dt}(t_i, \mathbf{w}_1^o) - f_1(t_i, \Psi_1, \Psi_2) \right)^2 + \left(\frac{d\Psi_2}{dt}(t_i, \mathbf{w}_2^o) - f_2(t_i, \Psi_1, \Psi_2) \right)^2 \right),\tag{35}$$

where

$$\begin{aligned}f_1 &= \alpha_2 + t_i N_2(t_i, \mathbf{w}_2^o), \\ f_2 &= \mu(1 - (\alpha_1 + t_i N_1(t_i, \mathbf{w}_1^o))^2)(\alpha_2 + t_i N_2(t_i, \mathbf{w}_2^o)) - (\alpha_1 + t_i N_1(t_i, \mathbf{w}_1^o)).\end{aligned}$$

We carried out numerical experiments within a wide range of values of the parameter μ that controls the stiffness, namely from $\mu = 1$ to $\mu = 100000$, using a constant grid of $n = 60$ equidistant points in the interval $[0, 6]$ for the proposed machine learning scheme. For the sake of presentation, in the following Tables, we show here only the results obtained for $\mu = 1, 5, 6, 10, 100, 1000, 10000, 100000$, which are representative of the behaviour of the methods, while in the following Figures we show only the solutions obtained for $\mu = 1, 5, 6, 10$, where steep gradients arise; for $\mu > 10$ the solutions become flatter in the interval of interest $[0, 6]$. As with the ROBER problem, we tested the numerical performance of the proposed method against ode45 and ode15s. Here, for implementing our scheme, we set $n = 60$, $h = 600$ and hence $\bar{s} \simeq 0.01$, and tested its performance using two values for the tolerance tol , i.e. 10^{-2} and 10^{-3} . For comparison purposes, we used the same values of both the absolute and relative error tolerances for the functions ode45 and ode15s. The reference solution was computed using ode15s with tolerances equal to 10^{-8} . The resulting approximated solutions for $\mu = 1, 5, 6, 10$ are depicted in Figure 2 for the tolerance of 10^{-2} and in Figure-3 for 10^{-3} . The corresponding approximation errors for the various values of the parameter μ , in terms of the L_2 -norm, the L_∞ -norm of the error and in terms of the MAE, are reported in Tables 7-10. Again, the errors in these tables were computed using the grid points chosen to train the proposed RPNN. In Table 11, we provide the number of points required by each method and in Tables 12- 13, we report the corresponding execution times (median, 5th percentile and 95th percentile) for the tolerances of 10^{-2} and 10^{-3} , respectively, including the time required to compute the reference solution, for various values of the parameter μ . Finally, in Tables 14- 17, we depict the errors in the approximate solutions obtained with both tolerances, evaluated at 1000 equidistant points in $[0, 6]$. As in the case of the ROBER problem, for ode45 and ode15s the values of the solutions at these points were obtained by using the MATLAB function `deval`.

As shown, for the case when tolerances are set to 10^{-2} and for relatively small values of μ (indicatively, $\mu < 10$), the proposed machine learning scheme outperforms ode15s in all metrics, while its performance is comparable to the one obtained with ode45 (see Tables 7-8). It is worthy to note that for small values of μ , where the solution exhibits steep gradients in the specific time interval (e.g. for $\mu = 5, 6$), ode15s gives relatively large errors. Indicatively, for $\mu = 6$, the L_∞ -norm of the difference between the value of y_1 (y_2) computed by ode15s and the corresponding component of the reference solution at the end of the interval ($t = 6$), where a steep gradient arises, is $\|y_1 - y_1^{ref}\|_{L_\infty} \simeq 1$ ($\|y_2 - y_2^{ref}\|_{L_\infty} \simeq 4.29$), while the reference values is $y_1^{ref} \simeq -0.74$ ($y_2^{ref} \simeq -8.6$). That is, ode15s actually fails to adequately approximate the solution. The corresponding value of L_∞ -norm of the approximation errors resulting from the implementation of the proposed scheme is $\|y_1 - y_1^{ref}\|_{L_\infty} \simeq 0.13$ ($\|y_2 - y_2^{ref}\|_{L_\infty} \simeq 0.49$). On the other hand, when the value of the stiffness parameter is relatively small, ode45 results to considerably larger approximation errors when compared to our scheme. In particular, for $\mu = 1$, the L_{inf} -norm of the difference between the value of y_1 (y_2) provided by ode45 and the reference solution at the end of the interval is $\|y_1 - y_1^{ref}\|_{L_\infty} \simeq 0.13$ ($\|y_2 - y_2^{ref}\|_{L_\infty} \simeq$

0.14), with reference value $y_1^{ref} \simeq 1.27$ ($y_2^{ref} \simeq 2.44$). For $\mu = 1$, the corresponding norms obtained with the proposed scheme are $\|y_1 - y_1^{ref}\|_{L_\infty} \simeq 0.01$ ($\|y_2 - y_2^{ref}\|_{L_\infty} \simeq 0.004$). For larger values of the stiffness parameter (e.g. for $\mu > 100$) ode15s results to the best approximation accuracy; as shown, the proposed scheme achieves an adequate numerical accuracy ranging within the orders of 10^{-5} to 10^{-7} .

Interestingly enough, when the tolerances are set equal to 10^{-3} , we have a behaviour similar to the case when the tolerance is set to 10^{-2} . In particular, for solutions with steep gradients as in the case of $\mu = 6$, the proposed method provides better approximations when compared to ode15s and almost the same with ode45. For larger values of the stiffness parameter (e.g. for $\mu > 100$) ode15s results to the best approximation accuracy, yet, the proposed scheme achieves adequate numerical accuracy ranging between 10^{-5} and 10^{-7} .

This behaviour is also confirmed by the solutions evaluated at the 1000 equidistant points in the interval $[0,6]$ (see Tables 14- 17). Again, the execution times required by the RPNN method are larger than the times of the classical methods (see Tables 12-13), but the comments made for the ROBER problem apply also here. Thus, we conclude that our RPNN-based approach performs well in terms of accuracy regardless of the level of stiffness, combining in some sense the “good” properties of the other two solvers.

Table 7: van der Pol problem. L_2 -norm, L_∞ -norm absolute errors and MAE for y_1 of the solutions computed with tolerances set to 10^{-2} for different values of μ . The reference solution obtained with ode15s with tolerances set to 10^{-8} .

	L_2	L_∞	MAE	L_2	L_∞	MAE	L_2	L_∞	MAE
	$\mu = 1$			$\mu = 5$			$\mu = 6$		
RPNN	0.0279	0.0100	0.0023	0.1452	0.0902	0.0070	0.1652	0.1284	0.0066
ode45	0.5058	0.1740	0.0426	0.1261	0.0775	0.0067	0.1466	0.1136	0.0060
ode15s	0.1526	0.0577	0.0120	1.0596	0.6503	0.0548	1.5138	0.9542	0.0651
	$\mu = 10$			$\mu = 100$			$\mu = 1000$		
RPNN	0.0017	0.0006	0.0002	0.0003	6.60e-5	3.28e-5	9.01e-5	2.53e-5	9.92e-6
ode45	0.0017	0.0007	0.0002	0.0001	4.78e-5	1.57e-5	9.97e-6	3.77e-6	8.93e-7
ode15s	0.0179	0.0035	0.0020	0.0001	2.69e-5	9.49e-6	6.19e-8	1.68e-8	6.35e-9
	$\mu = 10000$			$\mu = 100000$					
RPNN	1.03e-5	2.49e-6	1.19e-6	6.59e-7	1.33e-7	7.99e-8			
ode45	1.04e-6	3.31e-7	9.34e-8	1.07e-7	3.68e-8	9.98e-9			
ode15s	1.45e-10	4.11e-11	1.51e-11	2.56e-12	7.01e-13	2.60e-13			

Table 8: van der Pol problem. L_2 -norm, L_∞ -norm absolute errors and MAE for y_2 of the solutions computed with tolerances set to 10^{-2} for different values of μ . The reference solution obtained with ode15s with tolerances set to 10^{-8} .

	L_2	L_∞	MAE	L_2	L_∞	MAE	L_2	L_∞	MAE
	$\mu = 1$			$\mu = 5$			$\mu = 6$		
RPNN	0.0450	0.0174	0.0045	0.7583	0.6028	0.0327	0.7030	0.4641	0.0245
ode45	0.4769	0.1993	0.0433	0.6919	0.5459	0.0281	0.5303	0.4275	0.0192
ode15s	0.3483	0.1321	0.0261	5.0013	3.0131	0.2172	6.6734	4.5342	0.2458
	$\mu = 10$			$\mu = 100$			$\mu = 1000$		
RPNN	0.0190	0.0123	0.0011	0.0045	0.0028	0.0003	0.0011	0.0003	9.21e-5
ode45	0.0290	0.0104	0.0025	0.0332	0.0106	0.0033	0.0299	0.0113	0.0027
ode15s	0.0017	0.0006	0.0002	1.38e-6	1.18e-6	8.52e-8	8.18e-10	1.43e-10	9.54e-11
	$\mu = 10000$			$\mu = 100000$					
RPNN	3.85e-5	2.44e-5	2.33e-6	4.06e-6	2.31e-6	2.92e-7			
ode45	0.0321	0.0103	0.0029	0.0308	0.0106	0.0028			
ode15s	5.58e-14	4.43e-14	4.06e-15	7.77e-16	1.26e-16	8.82e-17			

Table 9: van der Pol problem. L_2 -norm, L_∞ -norm absolute errors and MAE for y_1 of the solutions computed with tolerances set to 10^{-3} for different values of μ . The reference solution obtained with ode15s with tolerances set to 10^{-8} .

	L_2	L_∞	MAE	L_2	L_∞	MAE	L_2	L_∞	MAE
	$\mu = 1$			$\mu = 5$			$\mu = 6$		
RPNN	0.0258	0.0097	0.0021	0.1452	0.0905	0.0071	0.1727	0.1354	0.0069
ode45	0.0294	0.0111	0.0024	0.1402	0.0874	0.0068	0.1672	0.1311	0.0067
ode15s	0.0116	0.0032	0.0012	0.0350	0.0217	0.0018	1.0857	0.7257	
	$\mu = 10$			$\mu = 100$			$\mu = 1000$		
RPNN	0.0013	0.0006	0.0001	0.0012	0.0002	0.0001	8.39e-5	2.66e-5	9.28e-6
ode45	0.0013	0.0004	0.0001	9.42e-5	1.75e-5	1.13e-5	2.21e-6	6.35e-7	2.30e-7
ode15s	0.0074	0.0013	0.0009	0.0001	2.74e-5	9.94e-6	1.20e-7	2.91e-8	1.26e-8
	$\mu = 10000$			$\mu = 100000$					
RPNN	7.02e-6	1.43e-6	8.71e-7	1.39e-6	4.00e-7	1.49e-7			
ode45	1.19e-7	3.90e-8	1.16e-8	1.08e-8	3.49e-9	9.95e-10			
ode15s	6.47e-10	1.85e-10	6.54e-11	7.56e-12	1.89e-12	8.15e-13			

Table 10: van der Pol problem. L_2 -norm, L_∞ -norm absolute errors and MAE for y_2 of the solutions computed with tolerances set to 10^{-3} for different values of μ . The reference solution obtained with ode15s with tolerances set to 10^{-8} .

	L_2	L_∞	MAE	L_2	L_∞	MAE	L_2	L_∞	MAE
	$\mu = 1$			$\mu = 5$			$\mu = 6$		
RPNN	0.0477	0.0163	0.0044	0.7538	0.6015	0.0318	0.7301	0.4847	0.0254
ode45	0.0554	0.0198	0.0045	0.6954	0.5114	0.0288	0.6176	0.4947	0.0212
ode15s	0.0153	0.0051	0.0015	0.1711	0.1237	0.0075	4.6391	2.9251	0.1703
	$\mu = 10$			$\mu = 100$			$\mu = 1000$		
RPNN	0.0109	0.0090	0.0005	0.0050	0.0022	0.0004	0.0008	0.0003	6.65e-5
ode45	0.0029	0.0010	0.0003	0.0035	0.0011	0.0003	0.0036	0.0011	0.0003
ode15s	0.0009	0.0003	8.98e-5	5.27e-7	1.59e-7	5.37e-8	8.07e-10	1.55e-10	9.11e-11
	$\mu = 10000$			$\mu = 100000$					
RPNN	3.40e-5	2.19e-5	2.59e-6	1.41e-5	3.99e-6	1.23e-6			
ode45	0.0036	0.0011	0.0004	0.0032	0.0010	0.0003			
ode15s	2.99e-13	1.05e-13	2.62e-14	7.51e-16	1.30e-16	8.59e-17			

Table 11: van der Pol problem. Number of points required by ode45 and ode15s in the interval $[0,6]$ with tolerances 10^{-2} and 10^{-3} for various values of μ . The number of points used in the RPNN method were fixed to 60 regardless of the value of μ .

	μ	1	5	6	10	100	1000	10000	100000
$tol = 10^{-2}$	ode45	13	25	22	41	530	5410	54221	542336
	ode15s	35	52	33	20	19	20	21	23
$tol = 10^{-3}$	ode45	16	30	25	43	530	5411	54222	542336
	ode15s	54	71	65	28	24	22	23	24
	reference solution	356	455	301	146	99	87	66	49

Table 12: van der Pol problem. Median, 5th and 95th percentiles of the computational time (in seconds) for the different methods with tolerances set to 10^{-2} for various values of μ . The reference solution is computed with `ode15s` when tolerances equal to 10^{-8} .

	median	5th perc	95th perc	median	5th perc	95th perc	median	5th perc	95th perc
	$\mu = 1$			$\mu = 5$			$\mu = 6$		
RPNN	0.1578	0.1448	0.1960	0.2052	0.1806	0.2409	0.2269	0.2032	0.2854
<code>ode45</code>	0.0008	0.0007	0.0010	0.0009	0.0008	0.0013	0.0009	0.0008	0.0012
<code>ode15s</code>	0.0047	0.0042	0.0056	0.0081	0.0075	0.0097	0.0058	0.0053	0.0066
reference solution	0.0075	0.0068	0.0082	0.0139	0.0123	0.0161	0.0099	0.0087	0.0112
	$\mu = 10$			$\mu = 100$			$\mu = 1000$		
RPNN	0.1127	0.1060	0.1308	0.0744	0.0568	0.0868	0.0594	0.05264	0.1121
<code>ode45</code>	0.0012	0.0010	0.0016	0.0046	0.0040	0.0063	0.0421	0.0308	0.0719
<code>ode15s</code>	0.0029	0.0026	0.0037	0.0038	0.0032	0.0051	0.0040	0.0029	0.0075
reference solution	0.0049	0.0043	0.0068	0.0052	0.0044	0.0069	0.0057	0.0042	0.01163
	$\mu = 10000$			$\mu = 100000$					
RPNN	0.0280	0.0260	0.0385	0.0415	0.0373	0.0827			
<code>ode45</code>	0.3087	0.2972	0.3724	3.2564	3.0868	10.1607			
<code>ode15s</code>	0.0036	0.0034	0.0041	0.0053	0.0041	0.0147			
reference solution	0.0044	0.0042	0.0050	0.0053	0.0042	0.0156			

Table 13: van der Pol problem. Median, 5th and 95th percentiles of the computational time (in seconds) for the different methods with tolerances set to 10^{-3} for various values of μ . The reference solution is computed with `ode15s` when tolerances equal to 10^{-8} .

	median	5th perc	95th perc	median	5th perc	95th perc	median	5th perc	95th perc
	$\mu = 1$			$\mu = 5$			$\mu = 6$		
RPNN	0.2219	0.2134	0.2386	0.2886	0.2512	0.3487	0.2744	0.2651	0.2913
<code>ode45</code>	0.0010	0.0009	0.0012	0.0011	0.0010	0.0013	0.0010	0.0010	0.0012
<code>ode15s</code>	0.0069	0.0063	0.0088	0.0100	0.0095	0.0121	0.0099	0.0093	0.0115
	$\mu = 10$			$\mu = 100$			$\mu = 1000$		
RPNN	0.1467	0.1402	0.1579	0.0752	0.0706	0.0818	0.0554	0.0521	0.0623
<code>ode45</code>	0.0011	0.0011	0.0014	0.0043	0.0040	0.0053	0.0313	0.0286	0.0374
<code>ode15s</code>	0.0034	0.0031	0.0039	0.0036	0.0033	0.0041	0.0037	0.0032	0.0045
	$\mu = 10000$			$\mu = 100000$					
RPNN	0.0590	0.0551	0.0648	0.0410	0.0381	0.0452			
<code>ode45</code>	0.2915	0.2801	0.3639	2.9385	2.8654	3.3288			
<code>ode15s</code>	0.0037	0.0034	0.0050	0.0048	0.0044	0.0059			

6 Discussion

We developed a machine learning algorithm for the solution of ODEs with a focus on stiff ODEs. The proposed scheme combines the speed and the generalization advantages of RPNNs, the approximation capabilities of RBFs, and the effective way to choose trial solutions for ODE systems as described in [42]. In particular, we considered trial solutions of the form $\Psi_i(x, \mathbf{w}_i^o, \mathbf{p}_i) = \alpha_i + (x - x_0)N_i(x, \mathbf{w}_i^o, \mathbf{p}_i)$, fixing the parameters \mathbf{p}_i to deterministic and random values, thus reducing the dimension of the space where $N_i(x, \mathbf{w}_i^o, \mathbf{p}_i)$ is defined. The parameters \mathbf{p}_i also include the centers and the widths of the RBFs, and the random projections exploit the Johnson and Lindenstrauss Theorem [38] and universal approximation theorems that have been proved for ELMs [32].

Table 14: van der Pol problem. L_2 -norm, L_∞ -norm absolute errors and MAE for y_1 in the solution computed with tolerances set to 10^{-2} and then evaluated at 1000 equidistant points in $[0, 6]$

	L_2	L_∞	MAE	L_2	L_∞	MAE	L_2	L_∞	MAE
	$\mu = 1$			$\mu = 5$			$\mu = 6$		
RPNN	0.0518	0.0031	0.0014	0.0203	0.0028	0.0004	0.0271	0.0085	0.0002
ode45	1.9964	0.1684	0.0411	0.1226	0.0137	0.0018	0.0804	0.0206	0.0007
ode15s	0.6757	0.0648	0.0130	4.9310	0.7493	0.0624	6.3621	1.1378	0.0653
	$\mu = 10$			$\mu = 100$			$\mu = 1000$		
RPNN	0.0041	0.0007	7.44e-5	0.0010	0.0001	2.43e-5	0.0003	2.76e-5	9.55e-6
ode45	0.0064	0.0007	0.0001	0.0005	4.21e-5	1.08e-5	4.29e-5	4.00e-6	9.96e-7
ode15s	0.0783	0.0039	0.0021	0.0007	4.10e-5	1.99e-5	7.37e-6	3.94e-7	1.99e-7
	$\mu = 10000$			$\mu = 100000$					
RPNN	4.06e-5	2.49e-6	1.21e-6	2.69e-6	1.91e-7	8.17e-8			
ode45	4.43e-6	4.06e-7	1.03e-7	4.35e-7	4.09e-8	1.00e-8			
ode15s	3.41e-8	2.25e-9	7.55e-10	2.59e-11	1.71e-12	6.48e-13			

Table 15: van der Pol problem. L_2 -norm, L_∞ -norm absolute errors and MAE for y_2 in the solution computed with tolerances set to 10^{-2} and then evaluated at 1000 equidistant points in $[0, 6]$

	L_2	L_∞	MAE	L_2	L_∞	MAE	L_2	L_∞	MAE
	$\mu = 1$			$\mu = 5$			$\mu = 6$		
RPNN	0.0644	0.0055	0.0016	0.5489	0.0886	0.0071	0.5036	0.2196	0.0029
ode45	1.7833	0.1959	0.0401	0.3408	0.0759	0.0044	0.4607	0.0877	0.0046
ode15s	1.5799	0.1429	0.0289	23.0114	3.9790	0.2442	23.3323	4.2898	0.2040
	$\mu = 10$			$\mu = 100$			$\mu = 1000$		
RPNN	0.0834	0.0191	0.0010	0.1535	0.0368	0.0020	0.3264	0.0371	0.0060
ode45	0.1255	0.0117	0.0028	0.1326	0.0116	0.0030	0.1267	0.0110	0.0029
ode15s	0.0111	0.0035	0.0002	0.0009	0.0008	1.60e-6	4.21e-6	3.74e-6	6.04e-9
	$\mu = 10000$			$\mu = 100000$					
RPNN	0.1424	0.0369	0.0017	0.1462	0.0362	0.0021			
ode45	0.1313	0.0113	0.0030	0.1290	0.0113	0.0029			
ode15s	1.71e-8	1.71e-8	1.74e-11	1.18e-13	1.0256e-13	1.80e-16			

In this context, only the parameters w_i^o from the hidden to the output layer must be determined, and every hidden unit is “responsible” of learning the behaviour of the target function around a center point. The width of the RBF represents the width of the area which the hidden unit “learns” the solution. By applying this technique, we also avoid difficulties that come from the non-convexity of the optimization problems arising from nonlinear ODE problems and activation functions. Theoretical results guarantee the approximation capabilities of our RPNN, despite the much simpler way of obtaining the weights of the network. The results obtained show that the proposed machine learning approach is able to provide reasonably accurate numerical approximations to the solutions of the two benchmark stiff ODE problems, regardless of the stiffness level. We have shown that the proposed approach outperforms in terms of numerical accuracy the ode15s in cases where steep gradients arise in the solution, while it is more robust compared to the ode45 solver, which in generally needs more points to converge, or even fails to converge in some cases. Thus, the proposed scheme seems to combine the good approximation proprieties of the two widely used classical numerical methods (i.e. ode45 and ode15s). The computational times are greater than those resulting by the implementation of the ode45 and ode15s, but in our opinion this is mainly due to the fact our home-made code is not optimized (its optimization is out of the scope of the current work); however this is compensated by the fact that our method does not require the user to explicitly take into account the stiffness.

Possible future work includes the implementation of the scheme for the solution of large scale systems of stiff problems of ODEs as they arise from biological and/or chemical kinetics problems and its comparison with well established methods for solving medium to large scale stiff problems, the systematic investigation and selection of the random

Table 16: van der Pol problem. L_2 -norm, L_∞ -norm absolute errors and MAE for y_1 in the solution computed with tolerances set to 10^{-3} and then evaluated at 1000 points.

	L_2	L_∞	MAE	L_2	L_∞	MAE	L_2	L_∞	MAE
	$\mu = 1$			$\mu = 5$			$\mu = 6$		
RPNN	0.0413	0.0027	0.0011	0.0175	0.0028	0.0003	0.0111	0.0030	0.0001
ode45	0.0520	0.0040	0.0012	0.0245	0.0039	0.0003	0.0116	0.0031	0.0001
ode15s	0.0856	0.0103	0.0016	0.7425	0.1143	0.0089	4.6230	0.8923	0.0490
	$\mu = 10$			$\mu = 100$			$\mu = 1000$		
RPNN	0.0028	0.0007	5.60e-5	0.0044	0.0002	0.0001	0.0003	2.75e-5	8.76e-6
ode45	0.0006	6.87e-5	1.28e-5	4.52e-5	3.91e-6	1.03e-6	4.26e-6	3.79e-7	9.79e-8
ode15s	0.0354	0.0017	0.0010	0.0008	4.15e-5	2.07e-5	7.16e-6	3.87e-7	1.91e-7
	$\mu = 10000$			$\mu = 100000$					
RPNN	2.89e-5	1.96e-6	8.92e-7	4.91e-6	4.27e-7	1.32e-7			
ode45	4.39e-7	3.71e-8	1.02e-8	4.31e-8	3.78e-9	9.91e-10			
ode15s	3.56e-8	2.36e-9	7.78e-10	3.64e-11	1.82e-12	1.10e-12			

Table 17: van der Pol problem. L_2 -norm, L_∞ -norm absolute errors and MAE for y_2 in the solution computed with tolerances set to 10^{-3} and then evaluated at 1000 points.

	L_2	L_∞	MAE	L_2	L_∞	MAE	L_2	L_∞	MAE
	$\mu = 1$			$\mu = 5$			$\mu = 6$		
RPNN	0.0544	0.0044	0.0014	0.4845	0.0838	0.0058	0.5457	0.2403	0.0029
ode45	0.0951	0.0088	0.0021	0.1203	0.0247	0.0013	0.0702	0.0182	0.0007
ode15s	0.1423	0.0128	0.0029	3.6427	0.6554	0.0381	17.8947	3.5095	0.1523
	$\mu = 10$			$\mu = 100$			$\mu = 1000$		
RPNN	0.0520	0.0145	0.0005	0.1614	0.0328	0.0027	0.2422	0.0373	0.0044
ode45	0.0117	0.0011	0.0003	0.0132	0.0011	0.0003	0.0128	0.0011	0.0003
ode15s	0.0040	0.0008	8.85e-5	0.0001	0.0001	2.34e-7	8.60e-7	8.52e-7	1.11e-9
	$\mu = 10000$			$\mu = 100000$					
RPNN	0.1318	0.0357	0.0019	0.4102	0.0385	0.0080			
ode45	0.0131	0.0011	0.0003	0.0129	0.0011	0.0003			
ode15s	1.29e-11	8.80e-12	5.35e-14	9.51e-14	9.51e-14	1.03e-16			

distributions and their intervals that are used to set the parameters of the RBFs, the extension of the proposed scheme to the solution of time-dependent problems involving Partial Differential Equations, and its comparison with other physics-informed machine learning approaches that have been proposed for this task, such as Deep Learning (see, e.g., [47, 59, 61]) and other ELM-based schemes (see, e.g., [16, 17, 19]).

Acknowledgements

This work was partially supported by Gruppo Nazionale per il Calcolo Scientifico – Istituto Nazionale di Alta Matematica (GNCS-INdAM), Italy, and by the Italian program Fondo Integrativo Speciale per la Ricerca (FISR) - B55F20002320001.

Contribution Statement

All authors contributed equally to this work.

References

- [1] Achlioptas, D.: Database-friendly random projections: Johnson-Lindenstrauss with binary coins. *Journal of computer and System Sciences* **66**(4), 671–687 (2003)
- [2] Balaji, V., Priya, J.S., Kumar, J.D., Karthi, S.: Radial basis function neural network based speech enhancement system using SLANTLET transform through hybrid vector Wiener filter. In: *Inventive Communication and Computational Technologies*, pp. 711–723. Springer (2021)
- [3] Björck, r.: *Numerical methods for least squares problems*. Society for Industrial and Applied Mathematics (SIAM), Philadelphia, PA (1996)
- [4] Bottou, L., Curtis, F.E., Nocedal, J.: Optimization methods for large-scale machine learning. *SIAM Review* **60**(2), 223–311 (2018)
- [5] Broomhead, D.S., Lowe, D.: Radial basis functions, multi-variable functional interpolation and adaptive networks. Tech. rep., Royal Signals and Radar Establishment Malvern (United Kingdom) (1988)
- [6] Brugnano, L., Mazzia, F., Trigiante, D.: Fifty years of stiffness. In: *Recent advances in computational and applied mathematics*, pp. 1–21. Springer (2011)
- [7] Budkina, E., Kuznetsov, E., Lazovskaya, T., Tarkhov, D., Shemyakina, T., Vasilyev, A.: Neural network approach to intricate problems solving for ordinary differential equations. *Optical Memory and Neural Networks* **26**(2), 96–109 (2017)
- [8] Butcher, J.B., Verstraeten, D., Schrauwen, B., Day, C.R., Haycock, P.W.: Reservoir computing and extreme learning machines for non-linear time-series data analysis. *Neural Networks* **38**, 76–89 (2013)
- [9] Calabrò, F., Fabiani, G., Siettos, C.: Extreme learning machine collocation for the numerical solution of elliptic PDEs with sharp gradients. arXiv preprint arXiv:2012.05871 (2020)
- [10] Cao, W., Wang, X., Ming, Z., Gao, J.: A review on neural networks with random weights. *Neurocomputing* **275**, 278–287 (2018)
- [11] Cha, I., Kassam, S.A.: Channel equalization using adaptive complex radial basis function networks. *IEEE Journal on Selected Areas in Communications* **13**(1), 122–131 (1995)
- [12] Chakraverty, S., Mall, S.: Single layer Chebyshev neural network model with regression-based weights for solving nonlinear ordinary differential equations. *Evolutionary Intelligence* pp. 1–8 (2020)
- [13] Chen, S., Mulgrew, B., Grant, P.M.: A clustering technique for digital communications channel equalization using radial basis function networks. *IEEE Transactions on Neural Networks* **4**(4), 570–590 (1993)
- [14] Cybenko, G.: Approximation by superpositions of a sigmoidal function. *Mathematics of Control, Signals and Systems* **2**, 303–314 (1989)
- [15] Dasgupta, S., Gupta, A.: An elementary proof of a theorem of Johnson and Lindenstrauss. *Random Structures & Algorithms* **22**(1), 60–65 (2003)
- [16] Dong, S., Li, Z.: Local extreme learning machines and domain decomposition for solving linear and nonlinear partial differential equations. arXiv preprint arXiv:2012.02895 (2020)
- [17] Dong, S., Li, Z.: A modified batch intrinsic plasticity method for pre-training the random coefficients of extreme learning machines. arXiv preprint arXiv:2103.08042 (2021)
- [18] Dufera, T.T.: Deep neural network for system of ordinary differential equations: vectorized algorithm and simulation. *Machine Learning with Applications* p. 100058 (2021)
- [19] Dwivedi, V., Srinivasan, B.: Physics informed extreme learning machine (pielm)—a rapid method for the numerical solution of partial differential equations. *Neurocomputing* **391**, 96–118 (2020)
- [20] Er, M.J., Wu, S., Lu, J., Toh, H.L.: Face recognition with radial basis function (RBF) neural networks. *IEEE Transactions on Neural Networks* **13**(3), 697–710 (2002)
- [21] Fabiani, G., Calabrò, F., Russo, L., Siettos, C.: Numerical solution and bifurcation analysis of nonlinear partial differential equations with extreme learning machines. arXiv preprint arXiv:2104.06116 (2021)
- [22] Famelis, I.T., Kaloutsas, V.: Parameterized neural network training for the solution of a class of stiff initial value systems. *Neural Computing and Applications* **33**(8), 3363–3370 (2021)
- [23] Filici, C.: On a neural approximator to ODEs. *IEEE Transactions on Neural Networks* **19**(3), 539–543 (2008)
- [24] Gerstberger, R., Rentrop, P.: Feedforward neural nets as discretization schemes for ODEs and DAEs. *Journal of Computational and Applied Mathematics* **82**(1-2), 117–128 (1997)

- [25] Giryas, R., Sapiro, G., Bronstein, A.M.: Deep neural networks with random gaussian weights: A universal classification strategy? *IEEE Transactions on Signal Processing* **64**(13), 3444–3457 (2016)
- [26] Golub, G.H., Van Loan, C.F.: *Matrix computations*, third edn. Johns Hopkins University Press, Baltimore, MD (1996)
- [27] Hornik, K., Stinchcombe, M., White, H.: Multilayer feedforward networks are universal approximators. *Neural Networks* **2**(5), 359–366 (1989)
- [28] Hornik, K., Stinchcombe, M., White, H.: Universal approximation of an unknown mapping and its derivatives using multilayer feedforward networks. *Neural Networks* **3**(5), 551–560 (1990)
- [29] Huang, G., Zhou, H., Ding, X., Zhang, R.: Extreme learning machine for regression and multiclass classification. *IEEE Transactions on Systems, Man, and Cybernetics, Part B (Cybernetics)* **42**(2), 513–529 (2012)
- [30] Huang, G.B.: An insight into extreme learning machines: random neurons, random features and kernels. *Cognitive Computation* **6**(3), 376–390 (2014)
- [31] Huang, G.B.: What are extreme learning machines? Filling the gap between Frank Rosenblatt’s dream and John von Neumann’s puzzle. *Cognitive Computation* **7**(3), 263–278 (2015)
- [32] Huang, G.B., Chen, L., Siew, C.K., et al.: Universal approximation using incremental constructive feedforward networks with random hidden nodes. *IEEE Trans. Neural Networks* **17**(4), 879–892 (2006)
- [33] Huang, G.B., Zhu, Q.Y., Siew, C.K.: Extreme learning machine: theory and applications. *Neurocomputing* **70**(1-3), 489–501 (2006)
- [34] Husmeier, D.: Random vector functional link (RVFL) networks. In: *Neural Networks for Conditional Probability Estimation*, pp. 87–97. Springer (1999)
- [35] Igelnik, B., Pao, Y.H.: Stochastic choice of basis functions in adaptive function approximation and the functional-link net. *IEEE Transactions on Neural Networks* **6**(6), 1320–1329 (1995)
- [36] Jaeger, H.: Adaptive nonlinear system identification with echo state networks. *Advances in Neural Information Processing Systems* **15**, 609–616 (2002)
- [37] Jaeger, H., Haas, H.: Harnessing nonlinearity: Predicting chaotic systems and saving energy in wireless communication. *Science* **304**(5667), 78–80 (2004)
- [38] Johnson, W.B., Lindenstrauss, J.: Extensions of Lipschitz mappings into a Hilbert space. *Contemporary Mathematics* **26**(1), 189–206 (1984)
- [39] Karniadakis, G.E., Kevrekidis, I.G., Lu, L., Perdikaris, P., Wang, S., Yan, L.: Physics-informed machine learning. *Nature Reviews Physics* **3**, 422–440 (2021)
- [40] Kelley, C.T.: *Iterative methods for optimization*. SIAM (1999)
- [41] Kratsios, A.: The universal approximation property: characterizations, existence, and a canonical topology for deep-learning. arXiv preprint arXiv:1910.03344 (2019)
- [42] Lagaris, I.E., Likas, A., Fotiadis, D.I.: Artificial neural networks for solving ordinary and partial differential equations. *IEEE Transactions on Neural Networks* **9**(5), 987–1000 (1998)
- [43] Lambert, J.: *Numerical Methods for Ordinary Differential Systems: The Initial Value Problem*. Wiley (1992)
- [44] Lee, H., Kang, I.S.: Neural algorithm for solving differential equations. *Journal of Computational Physics* **91**(1), 110–131 (1990)
- [45] Liao, Y., Fang, S.C., Nuttle, H.L.: Relaxed conditions for radial-basis function networks to be universal approximators. *Neural Networks* **16**(7), 1019–1028 (2003)
- [46] Lu, L., Meng, X., Mao, Z., Karniadakis, G.E.: DeepXDE: a deep learning library for solving differential equations. *SIAM Review* **63**(1), 208–228 (2021)
- [47] Lu, L., Meng, X., Mao, Z., Karniadakis, G.E.: DeepXDE: a deep learning library for solving differential equations. *SIAM Review* **63**(1), 208–228 (2021)
- [48] Lukoševičius, M., Jaeger, H.: Reservoir computing approaches to recurrent neural network training. *Computer Science Review* **3**(3), 127–149 (2009)
- [49] Mall, S., Chakraverty, S.: Hermite functional link neural network for solving the Van der Pol–Duffing oscillator equation. *Neural Computation* **28**(8), 1574–1598 (2016)
- [50] Meade Jr, A.J., Fernandez, A.A.: The numerical solution of linear ordinary differential equations by feedforward neural networks. *Mathematical and Computer Modelling* **19**(12), 1–25 (1994)

- [51] Montazer, G.A., Giveki, D.: An improved radial basis function neural network for object image retrieval. *Neurocomputing* **168**, 221–233 (2015)
- [52] Ozturk, M.C., Xu, D., Principe, J.C.: Analysis and design of echo state networks. *Neural Computation* **19**(1), 111–138 (2007)
- [53] Pao, Y.H., Park, G.H., Sobajic, D.J.: Learning and generalization characteristics of the random vector functional-link net. *Neurocomputing* **6**(2), 163–180 (1994)
- [54] Pao, Y.H., Takefuji, Y.: Functional-link net computing: theory, system architecture, and functionalities. *Computer* **25**(5), 76–79 (1992)
- [55] Paquot, Y., Duport, F., Smerieri, A., Dambre, J., Schrauwen, B., Haelterman, M., Massar, S.: Optoelectronic reservoir computing. *Scientific Reports* **2**(1), 1–6 (2012)
- [56] Park, J., Sandberg, I.W.: Universal approximation using radial-basis-function networks. *Neural Computation* **3**(2), 246–257 (1991)
- [57] Pinkus, A.: Approximation theory of the MLP model. *Acta Numerica* **8**, 143–195 (1999)
- [58] Powell, M.J.: Radial basis functions for multivariable interpolation: a review. *Algorithms for Approximation* (1987)
- [59] Raissi, M., Perdikaris, P., Karniadakis, G.E.: Numerical gaussian processes for time-dependent and nonlinear partial differential equations. *SIAM Journal on Scientific Computing* **40**(1), A172–A198 (2018)
- [60] Raissi, M., Perdikaris, P., Karniadakis, G.E.: Physics-informed neural networks: a deep learning framework for solving forward and inverse problems involving nonlinear partial differential equations. *Journal of Computational Physics* **378**, 686–707 (2019)
- [61] Raissi, M., Perdikaris, P., Karniadakis, G.E.: Physics-informed neural networks: A deep learning framework for solving forward and inverse problems involving nonlinear partial differential equations. *Journal of Computational Physics* **378**, 686–707 (2019)
- [62] Renals, S.: Radial basis function network for speech pattern classification. *Electronics Letters* **25**(7), 437–439 (1989)
- [63] Robertson, H.: The solution of a set of reaction rate equations. *Numerical Analysis: an Introduction* **178182** (1966)
- [64] Sakemi, Y., Morino, K., Leleu, T., Aihara, K.: Model-size reduction for reservoir computing by concatenating internal states through time. *Scientific Reports* **10**(1), 1–13 (2020)
- [65] Schmidt, W., Kraaijveld, M., Duin, R.: Feedforward neural networks with random weights. In: *Proceedings 11th IAPR International Conference on Pattern Recognition. Vol.II. Conference B: Pattern Recognition Methodology and Systems*, pp. 1–4. IEEE Computer Society Press (1992)
- [66] di Serafino, D., Krejić, N., Krklec Jerinkić, N., Viola, M.: LSOS: line-search second-order stochastic optimization methods for nonconvex finite sums. *arXiv preprint arXiv:2007.15966* (2021)
- [67] Shampine, L.F., Reichelt, M.W.: The MATLAB ODE suite. *SIAM Journal on Scientific Computing* **18**(1), 1–22 (1997)
- [68] Tsoulos, I.G., Gavrilis, D., Glavas, E.: Solving differential equations with constructed neural networks. *Neurocomputing* **72**(10-12), 2385–2391 (2009)
- [69] Vempala, S.S.: *The random projection method*, vol. 65. American Mathematical Soc. (2005)
- [70] Venkateswarlu, R., Kumari, R.V., Jayasri, G.V.: Speech recognition using radial basis function neural network. In: *2011 3rd International Conference on Electronics Computer Technology*, vol. 3, pp. 441–445. IEEE (2011)
- [71] Verstraeten, D., Schrauwen, B., d’Haene, M., Stroobandt, D.: An experimental unification of reservoir computing methods. *Neural Networks* **20**(3), 391–403 (2007)
- [72] Wang, J.: Geometric structure of high-dimensional data. In: *Geometric Structure of High-Dimensional Data and Dimensionality Reduction*, pp. 51–77. Springer (2012)
- [73] Yadav, N., Yadav, A., Kumar, M., et al.: *An introduction to neural network methods for differential equations*. Springer (2015)
- [74] Yang, Y., Hou, M., Luo, J.: A novel improved extreme learning machine algorithm in solving ordinary differential equations by legendre neural network methods. *Advances in Difference Equations* **2018**(1), 1–24 (2018)

-
- [75] Zeelan Basha, C., Sai Teja, T., Ravi Teja, T., Harshita, C., Rohith Sri Sai, M.: Advancement in classification of X-ray images using radial basis function with support of Canny edge detection model. In: *Computational Vision and Bio-Inspired Computing*, pp. 29–40. Springer (2021)
- [76] Zemouri, R., Racoceanu, D., Zerhouni, N.: Recurrent radial basis function network for time-series prediction. *Engineering Applications of Artificial Intelligence* **16**(5-6), 453–463 (2003)
- [77] Zhang, L., Suganthan, P.N.: A comprehensive evaluation of random vector functional link networks. *Information Sciences* **367**, 1094–1105 (2016)

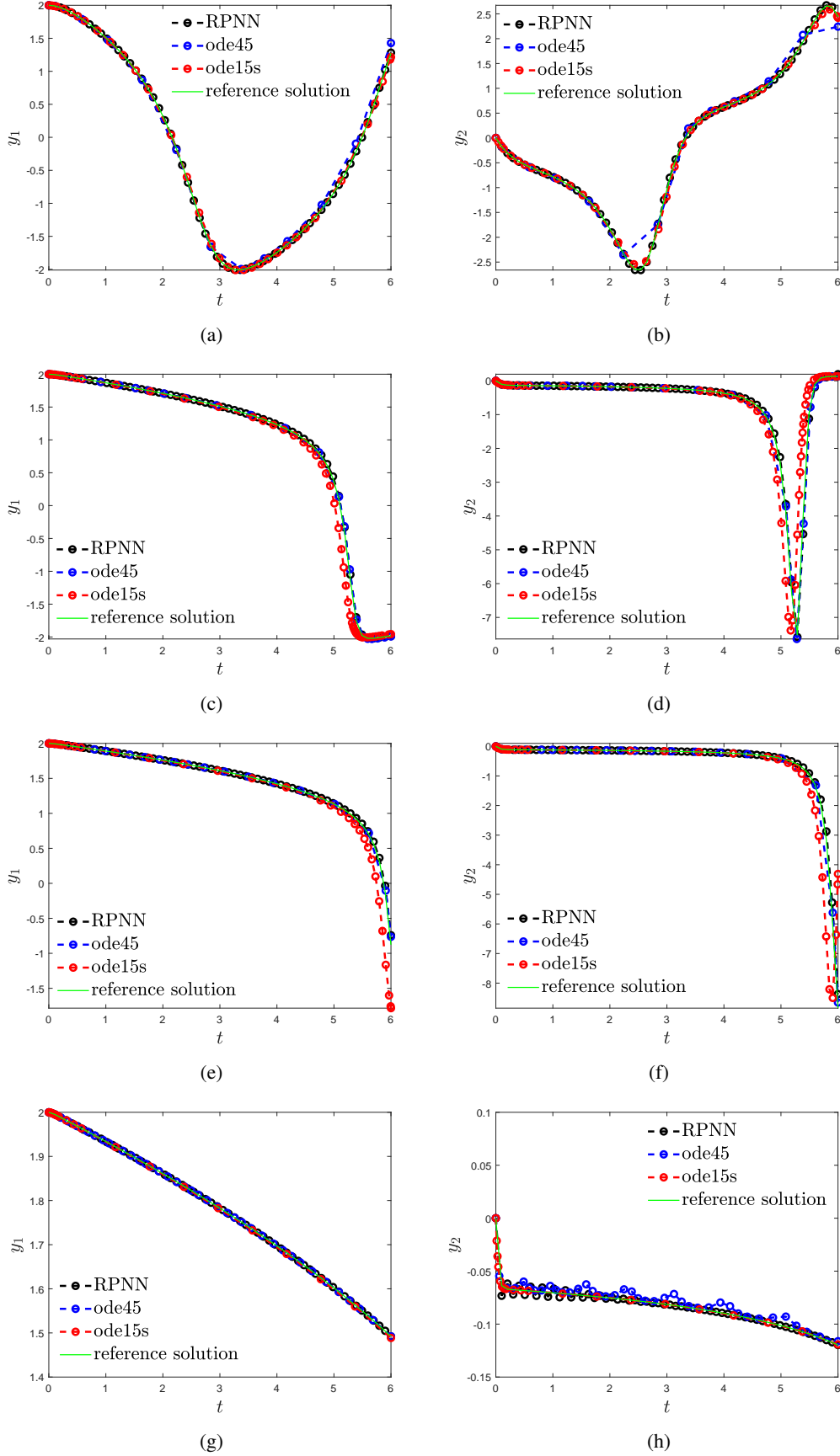


Figure 2: van der Pol problem. Approximate solutions computed by the different methods in the interval $[0, 6]$ with tolerances set to 10^{-2} for different values of μ for which steep gradients arise. $\mu = 1$: (a)-(b), $\mu = 5$: (c)-(d), $\mu = 6$: (e)-(f) and $\mu = 10$: (g)-(h). For $\mu > 10$ the solutions become flatter in the reference domain.

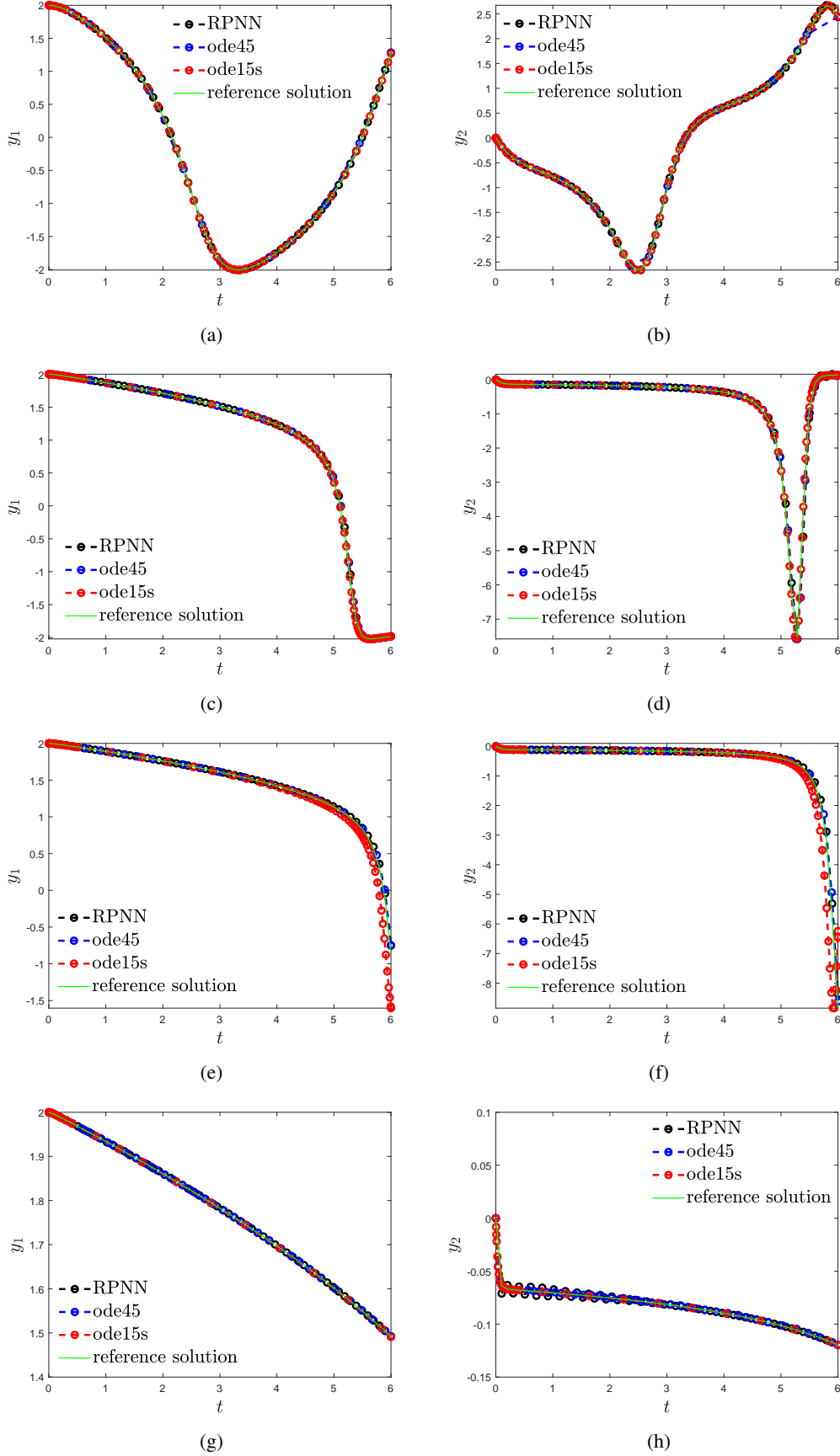


Figure 3: van der Pol problem. Approximate solutions computed by the different methods in the interval $[0, 6]$ with tolerances set to 10^{-3} for different values of μ for which steep gradients arise. $\mu = 1$: (a)-(b), $\mu = 5$: (c)-(d), $\mu = 6$: (e)-(f) and $\mu = 10$: (g)-(h). For $\mu > 10$ the solutions become flatter in the reference domain.